CONTENTS

From Editor

Engineering Faculty of Istanbul Aydın University has started to publish an international journal on Electronics, Mechanical and Mechatronics Engineering, denoted as "International Journal of Electronics, Mechanical and Mechatronics Engineering (IJEMME)". We have especially selected the scientific areas which will cover future prospective engineering titles such as Robotics, Mechanics, Electronics, Telecommunications, Control Systems, System Engineering, Biomedical, and Renewable Energy Sources.

We have selected only a few of the manuscripts to be published after a peer review process of many submitted studies. Editorial members aim to establish an international journal IJEMME, which will be welcomed by Engineering Index (EI) and Science Citation Index (SCI) in short period of time.

Prof. Dr. Zafer UTLU
Editor

A New Compact Circular Polarized CPW Antenna Design for UWB Application

Hemrah HIVEHCHI [1], Saeid KARAMZADEH*[2]

Abstract – Current paper proposes a new Coplanar waveguide (CPW) feed antenna for UWB application. The suggested antenna consists of a circular patch with two circular slots and a semicircular gap on the feedline with two rectangular shapes as ground in 2.6 x 30 x1.6mm³ dimensions with spiral and semicircular slots on it. In this outline, the impedance bandwidth (S11) has increased to a significate number together with the axial ratio bandwidth (ARBW), 123 % (3.3 GHz - 13.9 GHz). The article presents the designing steps of the antenna.

Keywords - *UWB, CP, CPW feed*

1. Introduction

Low specifications, low cost, light weight and being able to integrate with Monolithic Microwave Integrated Circuits (MMICs) for Ultra Wide Band application (UWB) would make a micro-strip slot antenna a good choice for so many applications [1,2]. Circularly Polarized (CP) antennas are more preferred in wireless communications, sensors, radio frequency identifiers (RFID), satellite communication and vehicular radar due to the elimination of multipath fading problem and the enhanced system performance [3,4]. Among feeding methods, coplanar waveguide (CPW) feed provides some advantages such as wideband, easy integration and single metallic layer [5]. Some of the methods for generating CP radiation studied in the literature are slots in the ground [6], S-shaped slots [7], feed networks composed of three Wilkinson power dividers [8], topology-based steps [9], feed positioning with E- and U-shaped slots [10], asymmetric T-shaped strip [11], two linked square slot-rings [12] and inverted L-slits on the ground.

UWB is currently used for receiving special attention and is quite an important topic in communication systems. UWB technology brings the facilities and mobility of wireless communications to high speed inter connects in devices throughout the digital anywhere. Providing wireless connection of multiple devices for the transmission of video, audio and other high bandwidth data, UWB is the mostly preferred technology for freeing people from wires. UWB short-range radio technology supplements other longer-range radio technologies such as Wi-Fi, WiMAX and cellular wide area communications. It is used for connecting data from a host device to other devices in the immediate area (up to 10 m or 30 feet) [13]. Today, antenna designing for UWB systems is a big challenge for the researchers.

Current study presents a new design of a CPW fed Circularly Polarized Square slot antenna by partially improving and combining previous methods for obtaining a better result. Based on the simulated results, the impedance bandwidth is about 123 % and the 3 dB AR bandwidth is about 32 %. Proposed antenna will support an UWB application of which the frequency range is defined as: 3.1-10.6 GHz or fractional bandwidth more than 109 %.

[1]Department of Electrical and Electronics Engineering, Istanbul Aydin University, Istanbul, Turkey
[2]Application & Research Center for Advanced Studies, Istanbul Aydin University, Turkey hemrahhivehchi@stu.aydin.edu.tr, karamzadeh@itu.edu.tr

2. Antenna Design

This section is divided in four parts to better describe the proposed antenna designing process in steps. In all the steps, antennas were designed on a commercially cheap FR4-epoxy substrate with ε_r =4.4 and tan (δ) = 0.024, and the feedline of the proposed antennas were CPW which is designed for connecting to a 50 Ω SMA connector.

2.1 Antenna I

The first step simulates the proposed antenna with the circular patch and CPW feed. The configuration of the provided antenna is shown in Figure 1(a). In this section, we attempt to tune the impedance band on 50 ohms with gaps besides the feed line and grounds. For designing and finding the improved parameters we have utilized the Ansoft High Frequency Structure Simulator Software (HFSS, ver.16). For the predigesting in the antenna design G = 26 mm, L = 30 mm, h = 1.6 mm measurements were selected. Figure 1(b) and (c) have shown results of S11 and AR for the particular antenna. The results are acceptable for S11 (2.2, unlimited) but not for Circular Polarization (CP) therefore AR must be improved for this antenna. The parameters of the antenna are as follows: G = 2.6, L = 30, h = 1.6, r1 = 8, L1=12, L2 = 8, L3 = 12.5, L4 = 7, L5 = 9, L6 = 5.5, L7 = 4.5, L8 = 4.9, L9 = 2, L10 = 14.4, L11 =9, L12=3.5and W1 = 2.5, W2 = 2.1, (All units are given in millimeters).

(a)

(b)

(c)
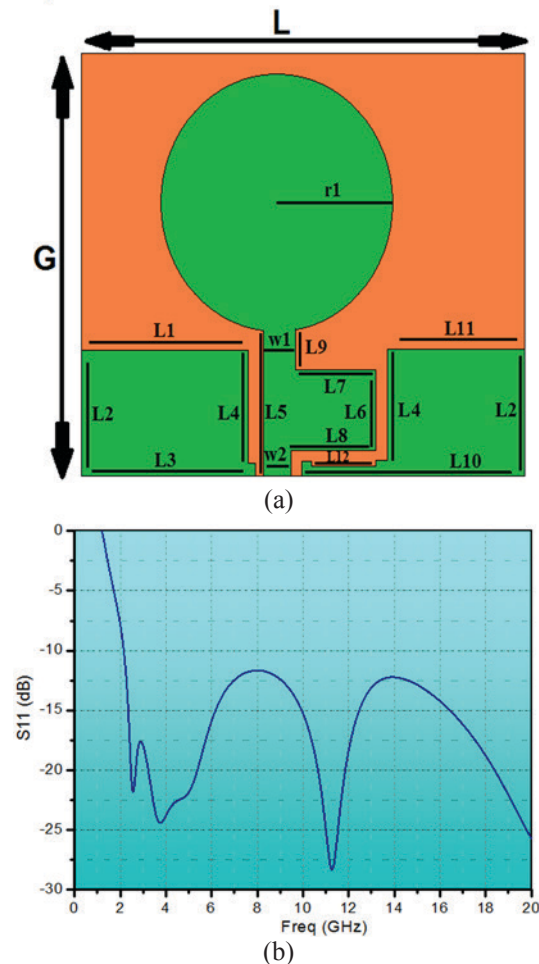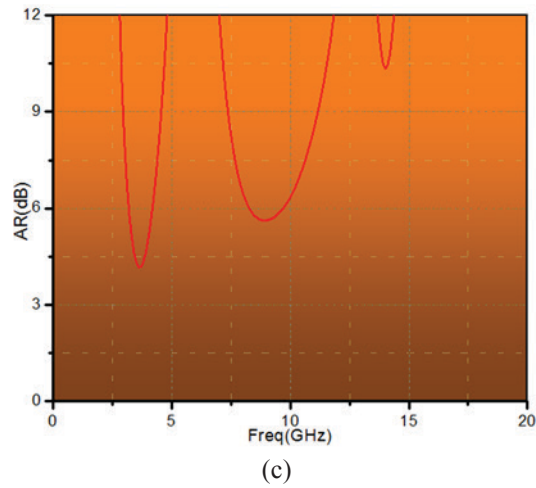
Figure 1. (a) Configuration of the antenna I, (b) S11and (c) AR for antenna I

2.2. Antenna II

In this step, the AR is improved by two circular gaps on the patch. The antenna configuration and the results of the antenna II are shown in Figure 2. According to the impedance band -10 dB s11 graphs from Figure 2(b), the operation frequency starts from 2 GHz, which is a good result and proper for UWB application as well. However, 3-dB AR graph in Figure 2(c) shows that it can be improved for a better performance in Circularly Polarized Mode. The diameters of circular gaps are r2=6.5mm and r3=4.5mm.

(a)

(b)

(c)
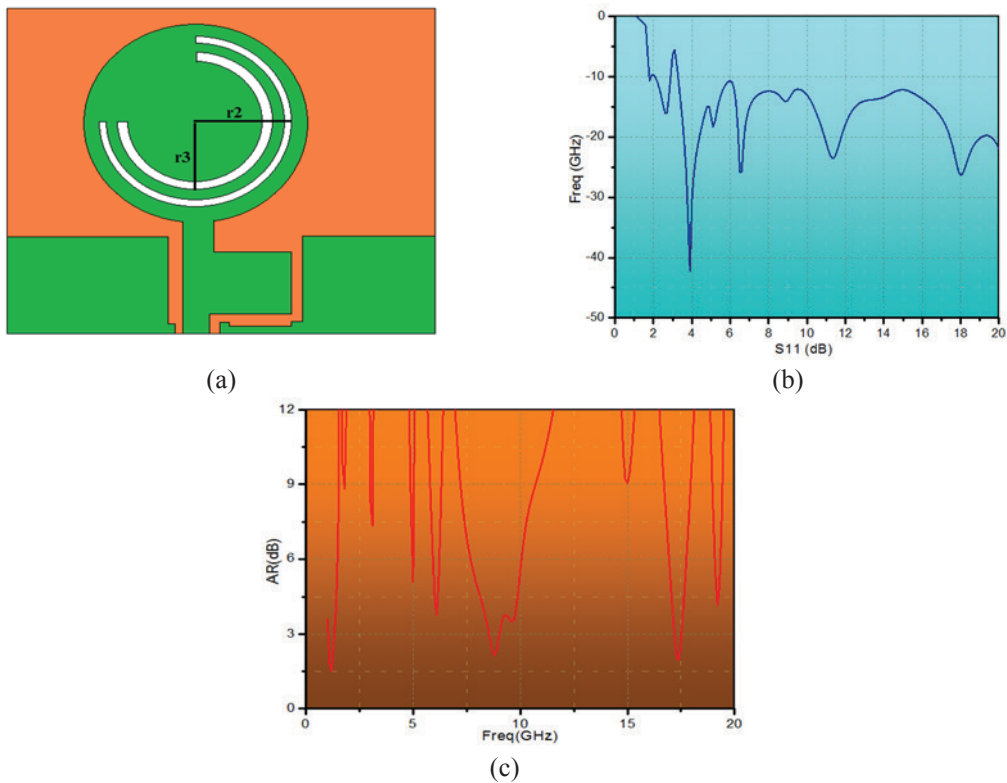
Figure 2. (a) Configuration of the antenna II, (b) S11and (c) AR for Antenna II

2.3 Antenna III

This step utilizes spiral gap and semicircular shapes in the ground stepping up the ground and patch for the improvement of the AR. The antenna configuration and results of the antenna III are shown in Figure 3. The parameters are l1=5.5, l2=5, l3=3.5, l4=3.5, l5=2, l6=2, l7= 3, l8=2.5 (all in mm).

(a)   (b)

(c)
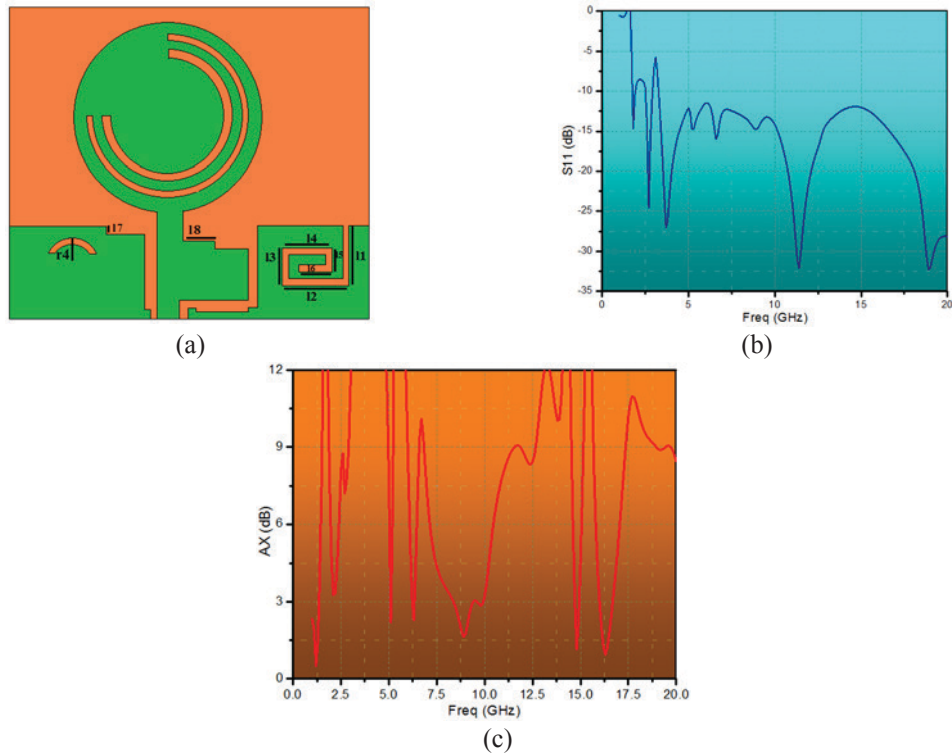
Figure 3. (a) Configuration of the antenna III, (b) S11and (c) AR for antenna III

2.4 Antenna IV

Finally, with a C shaped feed line and more stepped up in ground, Antenna IV design has given better results regarding AR. The configuration and the results of the proposed antenna (i.e. the final step of the antenna designing process) are shown in Figure 4 (r5 is 2 mm). Figure 5 shows the 3-D radiation pattern and antenna maximum gain (6.7dB). Right Hand Circularly Polarization (RHCP) and Left Hand Circularly Polarization (LHCP) radiation pattern for spatial frequency and different degrees are shown in Figure 6. In comparison with the recently published related works, the antenna performances such as impedance bandwidth, axial ratio and gain has improved in this study. Besides, the size of the antenna has been reduced impressively. Table 1 shows a comparison of the proposed antenna with the related work.

(a)

(b)

(c)
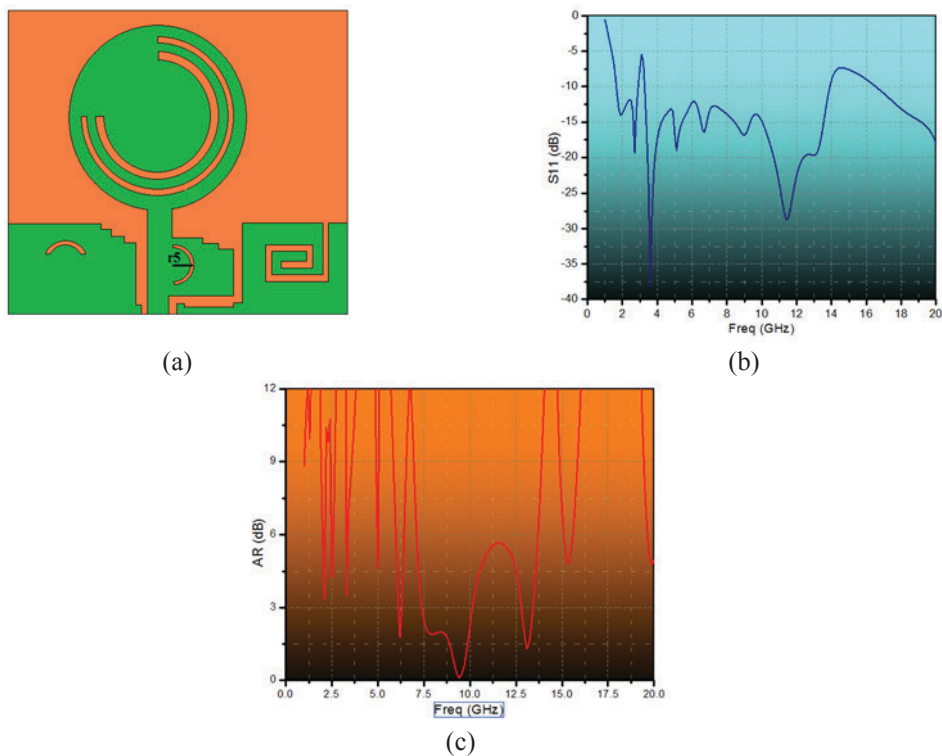
Figure 4. (a) Configuration of the proposed antenna, (b) S11 and (c) the AR of the proposed antenna
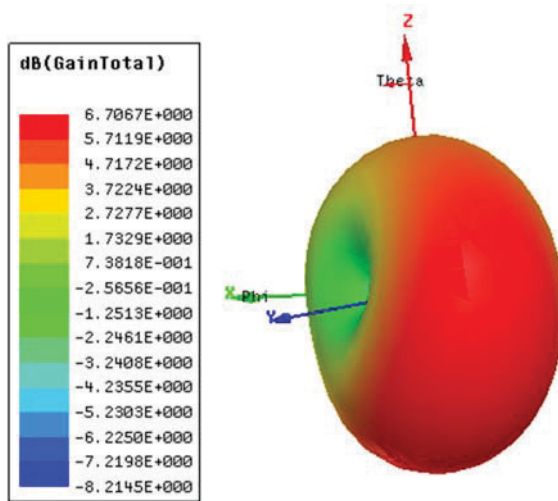
Figure 5. 3D radiation pattern

(a)   (b)

(c)   (d)
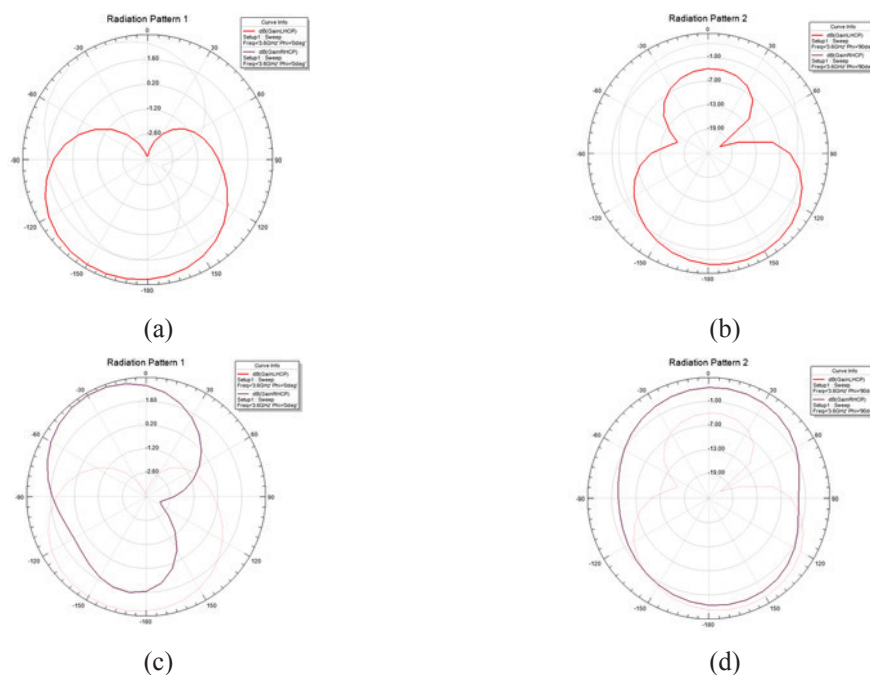
Figure 6. Simulated radiation patterns of the proposed antenna at (a) 3.6 GHz, 0 degree (b) 3.6 GHz,90 degrees for left hand and (c) 3.6 GHz, 0 degree (d) 3.6 GHz,90 degrees for right hand

Table 1. A comparison of the characteristics of some antennas with the proposed work (BW: Impedance Bandwidth and P.A: Proposed Antenna)

References	Gain	BW	Size
	(dB)	(GHz)	mm^3
[3]	4	1.6-3.05=52%	60x60x0.74
[14]	4.5	3-10.1=108%	60 x 60x0.8
[15]	4.32	2.6-13.1=132%	60 x 60x0.8
[16]	3.4	2.02-3.4=51.4%	60 x 60x0.8
P.A	6.7	3.3-13.9=123%	26 x 30x1.6

3. Conclusion

Current study proposes a new CP antenna presenting the designing steps and result improvement in this paper. The simulated results demonstrate that the proposed antenna has an impedance bandwidth of about 10.6 GHz (123 %) and a 3 dB AR bandwidth of about 1.8 GHz (32 %). Furthermore, the significant reduction in size is another novelty that the proposed antenna brings.

References

[1]   S. Karamzadeh, V. Rafii, M. Kartal, H. Saygin, "Compact UWB CP square slot antenna with two corners connected by a strip line" Electronics Letters, Vo. 52, Issue.1, pp: 10-12, Nov 2015.

[2]   Saeid Karamzadeh, Mesut Kartal, Sedef Kent, A Abed Ashtiyani, "Optimal Signal Processing Method in UWB Radar for Hidden Human Detection" EUSAR 2014; 10th European Conference on Synthetic Aperture Radar; pp: 1 - 3 Berlin, Germany, June 2014.

[3] J. Y. Sze and C. C. Chang, "Circularly polarized square   slot antenna with a pair of inverted-L grounded strips," *IEEE Antennas Wireless Propag. Lett.*, vol. 7, pp. 149-151, 2008.

[4] N. M. Jizat, S.K.A. Rahim, Y.C.Lo, M. M. Mansor "Compact Size of CPW Dual-Band Meander-Line Transparent Antenna for WLAN Applications" *IEEE*, Dec 2014

[5] C. C. Chou, K. H. Lin, and H. L. Su, "Broadband circularly polarised cross-patch-loaded square slot antenna," *Electron. Lett.*, vol. 43, no. 9,pp. 485–486, Apr. 26, 2007.

[6] G. Li, H. Zhai, T. Li, L. Li, and C. Liang, "A   compact antenna with broad band width and quad-sense circular polarization," *IEEE Antennas Wireless Propag. Lett.*, vol. 11, pp. 791–794, 2012.

[7] G. Li, H. Zhai, T. Li, L. Li, and C. Liang, "CPW-fed S-shaped slot antenna for broad band circular polarization," *IEEE Antennas Wireless Propag. Lett.*, vol. 12, pp. 619–622, 2013.

[8] Y. J. Hu, W. P. Ding, W. M. Ni, and W. Q. Cao, "Broadband circularly polarized cavity-backed slot antenna array with four linearly polarized disks located in a single circular slot," *IEEE Antennas Wireless Propag.Lett.*, vol. 11, pp. 496–499, 2012.

[9] J. Oh and K. Sarabandi, "A topology-based miniaturization of circularly polarized patch antennas," *IEEE Trans. Antennas Propag.*, vol. 61, no. 3, pp. 1422–1426, Mar. 2013.

[10] Y. Chen and C. Wang, "Characteristic-mode-based improvement of circularly polarized U-slot and E-shaped patch antennas," *IEEE Antennas Wireless Propag. Lett.*, vol. 11, pp. 1474–1477, 2012.

[11] S. Pan, J. Sze, and P. Tu, "Circularly polarized square slot antenna with a largely enhanced axial-ratio bandwidth," *IEEE Antennas Wireless Propagation Lett.*, vol. 11, pp. 969–972, 2012.

[12] T. Chang and J. Lin, "Circularly polarized antenna having two linked slot-rings," *IEEE Trans. Antennas Propag.*, vol. 59, no. 8, pp. 3057–3060, Aug. 2011.

[13] Y. Rahayu1, T. Abd. Rahman1, R. Ngah1, P.S. Hall, "Ultra Wideband Technology and Its Applications," *IEEE Antennas Wireless Propag. Lett.*, pp. 978-1-4244, 2008.

[14] S. Karamzadeh and H. Hivehchi "A New CPW-Fed Circularly Polarized Square Slot Antenna Design," IU-Journal of Electrical & Electronics Engineering*, under publish.

[15] J. Pourahmadazar, C. Ghobadi, J. Nourinia, N. Felegari, and H. Shirzad., "Broadband CPW-Fedcircularly polarized square slot antenna with inverted-L strips for UWB applications," *IEEE Antennas Wireless Propag.*

[16] J. Y. Sze, C. I. G. Hsu, Z. W. Chen, and C. C. Chang, "Broad band CPW-fed circularly polarized square slot antenna with lightening-shaped feedline and inverted-L grounded strips," IEEE Trans. Antennas Propag., vol. 58, no. 3, pp. 973–977, Mar. 2010.

Data Fusion-Based Multimodal Biometric System for Face Recognition Using Manhattan Distance Penalty Weight

Bilal Ahmed[1], Taner Cevik*[2], Nazife Cevik[3]

Abstract - In this paper, we propose a multimodal biometric face recognition technique which is mainly based on the 2D Discrete Wavelet Transform (DWT) and Data Fusion (DF) and utilizes data fusion techniques at the score level of the system algorithm. The technique employs three discrete unimodal feature extraction and classification methods. The first two feature vectors are generated from raw images by using Principal Component Analysis (PCA) and Local Binary Pattern (LBP) methods. During the generation of the third feature vector, images are initially transformed into the DWT domain. In result, approximation, vertical, horizontal and diagonal detail matrices are combined to form a Joint Feature Vector (JFV). K-Nearest Neighbor (KNN) classifier algorithm is separately applied to the three generated feature vectors to compute different score values for the same individual. These raw score values are fused together using a newly proposed data fusion technique based on Manhattan Distance Penalty Weighting (MDPW). The proposed MDPW penalizes an individual for scoring low points and further pushes it away from the potentially winning class before data fusion is conducted. The proposed approach was implemented on ORL and YALE public face databases. The results of the proposed approach are evaluated using the recognition rates and receiver operating characteristics of the biometric classification systems. Experimental results show that the proposed multimodal system performs better than the unimodal system and other multimodal systems that use different data fusion rules (e.g. Sum Rule or Product Rule). In ORL database, the recognition rate of up to 97% can be achieved using the proposed technique.

Keywords - *Face recognition, discrete wavelet transform, principal component analysis, discrete wavelet transform, local binary pattern, data fusion, Manhattan distance, k-nearest neighbor (KNN)*

1. Introduction

The need for a reliable system which is capable of establishing genuine peoples' and impostors' identities has snowballed over the years, especially with the increase in the global trend of crimes. These needs spurred active research in the field of biometrics. Over the years, imposters have been looking for loopholes that exist in the unimodal biometric system to fake identity leading to breach of privacy and security. The multimodal biometric system seeks to alleviate some of the drawbacks encountered by the unimodal biometric system. This improvement is achieved by consolidating the evidences presented by multiple biometric traits or sources. This system significantly improves the recognition performance, increases the degree of freedom and reduces spoof attacks and failure-to-enroll rate [1-3].

Advanced research on challenges related to the automatic identity establishment in individuals has been of keen interest to both governments and corporate organizations all around the world. With an increasing global integration of nations' economies and bilateral relationships, the need for tracking economic activities, social movements of individuals and forestalling crimes become equally important. One of the key platforms which frequently addresses some of these global challenges is the area of biometric systems [4].

[1] *Istanbul Aydin University, Florya, Istanbul, Turkey*

[2] *Istanbul Aydin University, Florya, Istanbul, Turkey, tanercevik@aydin.edu.tr*

[3] *Istanbul Arel University, Tepekent-Buyukcekmece, Istanbul, 34537, Turkey*

One of the key perspectives explored by recent researches in this regard is the use of more than one biometric trait or data from an individual for representation in the system. This method, usually referred to as a multimodal biometric system, may combine data of the same person from different biometric traits (e.g. Fingerprint and face), or use different algorithms on the same trait to arrive at a more robust representation of the individual in the biometric system [5-6]. In a situation where the multimodal system exploits different algorithms, more flexibility is added whereby the data fusion techniques implemented at different levels of the algorithm stages (e.g. Feature extraction level, score level, decision level). The evidence in literature indicates that the multimodal system significantly improves the performance of the unimodal biometric systems [6-7].

A comprehensive literature review on multimodal biometric systems was compiled by Ross et al. [8]. They extensively investigated different fusion schemes at score level. Also in ISO/IEC Technical Report, many explanations and analyses on the recent developments regarding various multimodal biometric fusions have been compiled. There are various researches on different levels of fusion in multimodal biometric systems. An approach based on mosaicking scheme was proposed by Ratha et al. [9]. They have constructed a combination of fingerprint samples from many other samples as the user rolls over his finger over the sensor surface area. Singh et al. [10] developed a multimodal face recognition system by fusing images from visible and thermal Infrared (IR) cameras at different levels. Kong et al. described the performance of a multimodal recognition system based on a fusion of thermal infrared camera and visible light camera samples [11]. Authors in [12] performed a fusion of iris and face at the feature level. In [13] fusion at feature level was conducted on hand and faces data. The process is done in three different phases. Authors in [14] proposed a platform for fusing classifiers and discussed the various methods involved in the combination schemes. In [15], authors study the performance comparison of score level fusion using three different classifiers that are the k-nearest-neighbor (k-NN) classifiers, decision trees, and logistic regression.

In this paper, a different approach is proposed for the multimodal biometric system. The technique considers data fusion at score level of the classifier but instead of using different classifiers for each unique feature evidence (as is the case in literature), the same classifier is used with the same normalization algorithm. Three feature extractions were used to present different biometric pieces of evidence from the same trait. Using DWT, a new feature extraction was introduced whereby the four representation from the DWT were concatenated, and the Principal Component Analysis (PCA) was used to extract final reduced features from the concatenated DWT features. Similarly, a method for fusion scores from a unimodal biometric system was proposed based on the Manhattan distance penalty weighting. Scores of the individual are penalized based on their weighted distance from the supposed winning class before fusion.

The rest of the paper is organized as follows: Section II provides literature background on the PCA, DWT, LBP and K-NN. Section III presents and discusses the proposed multimodal system using the proposed data fusion. Section IV clarifies the results of the simulations. Finally, Section V contains the conclusion on our findings and observations.

2. Preliminaries

The feature extraction and classifier algorithms are the most important factors in the overall success of the system. Hence, the choice of these feature extractors and classifiers become pertinent. In this section, a background that is used from the build-up to the proposed approach on these algorithms is presented as the preliminaries.

2.1 Principal Component Analysis (PCA)

The PCA algorithm tries to extract salient features from a vector that best represents a class to which that vector belongs [16-20]. The algorithm forms a Difference Matrix (DM) by subtracting the average of all the training set from each sample (vector) and concatenating the results. It then statistically computes the covariance of the DM and finds its eigenvectors and eigenvalues. This information (eigenvectors, DM) is used for projecting all the vectors into a vector space which best represents their class. For eigen-face approach, the projected vector space is used as a feature to represent a subject [21]. Figure 1 describes the PCA algorithm steps.
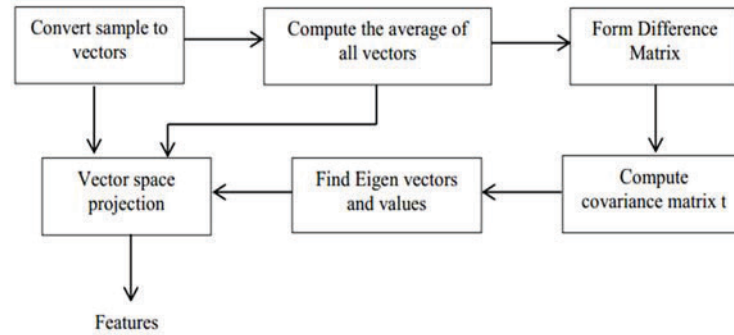
Figure 1. Block diagram of PCA feature extraction

2.2 Local Binary Pattern (LBP)

Due to its simplicity, LBP has been successfully applied in many applications. It uses *3x3* windows of the neighborhood pixels in the image to determine the new value of the center pixel that is under consideration [22]. Taking Figure 2 into account, initially the algorithms probe all the 8-neighborhood pixels around pixel I (z); any pixel greater than I (z) is assigned binary value *1* while those whose values are less than or equal to I (z) are assigned the bit value of *0*. *8-bit* code which is generated and converted to decimal for finding the new value of I(z). The procedure is applied to all the pixels in the image as the window slides from the top-left corner to the bottom-right corner of the image. In the end, each pixel's gray intensity is replaced by the *8-bit* code generated by the algorithm using local surrounding pixel information. The code is arranged clock or anti-clockwise consistently throughout the operation and then each code is converted back to a decimal integer. Figure 2 demonstrates how the algorithm operates.

100	240	30		0	1	0
20	I(z)=120	185	$\rightarrow$	0		1
70	100	200		0	0	1

Figure 2. LBP feature extraction

2.3 Discrete Wavelet Transform (DWT)

DWT is one of the multi-resolution signal and image processing algorithms. It tries to view signal or image at different resolutions so that features that cannot be seen at one resolution can be detected in another resolution. Two orthogonal or bi-orthogonal filters are used for achieving the transformation. One of the filters is high pass (Hi) while the other is Low pass (Lo). DWT can be seen as a departure from the famous Fourier Transform (FT) whose basis function is sinusoids. DWT is based on small waves that are called wavelets of varying frequency and limited duration [22].

DWT employs a scaling function to create a series of approximation of functions (images) each differing by a factor of 2 in resolution from its neighboring approximation. Additional functions which called wavelets encode the difference between adjacent approximations. Figure 3 shows how DTW features can be extracted. The last four wavelets are vectorized and fused using the sum rule to obtain the feature vector for that sample [22-27].

The 2D-DWT, on the other hand, is an extension of the one-dimensional discrete wavelet transform [28]. At a time, it simply functions in one dimension by evaluating the columns and rows of an image in a distinct way. In the initial stage, an analysis filter is applied to the rows of the input image. The convolution operation produces two sets of images where one set of the images are contained in its coarse row coefficients section whereas the other set of

images are stored in its row detail coefficients. The other set of analysis filters is applied to the columns of each of the input image. This operation produces four different images called sub-bands, wavelets or sub-images. Usually, the columns and rows that are analyzed with a high pass filter are designated with a symbol H. Likewise, those columns and rows that are analyzed with a low pass filter are designated with a symbol L. For instance, if a sub-image was obtained from convolution with a high pass filter on its rows and a low-pass filter on its columns, it is referred as (HL) sub-band. As a result, four wavelets are produced; approximate wavelet (A), horizontal wavelet (H), vertical wavelet (V) and the diagonal wavelet (D) as shown in Figure 3.
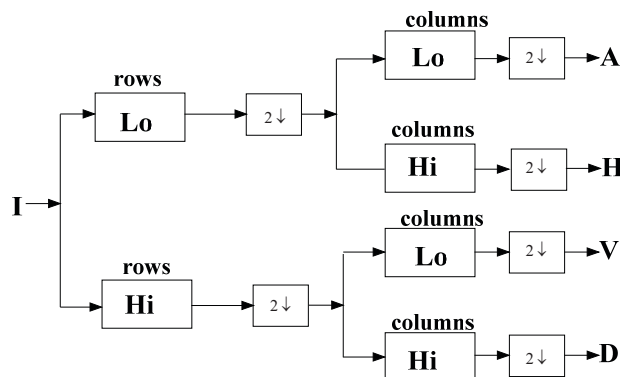
Figure 3. DWT decomposition process

2.4 K-Nearest Neighbor (K-NN)

K-NN can be described as a sort of instance-based learning or passive learning algorithm whereby the function is only approximated locally, and all computation is deferred until classification. The k-NN algorithm is among the simplest of all machine learning algorithms. Both for classification and regression, it can be useful to assign weights to the contributions of the neighbors so that the nearer neighbors contribute more to the average than the more distant ones. For example, a common weighting scheme consists in giving each neighbor a weight proportional to its closeness or otherwise to the test data. To compute the distance between a test vector and the training set vector distance metric algorithms such as Euclidean distance (l_2-norm), Manhattan Distance (l_1-norm), etc. are frequently used. Eq. (1-2) show how the distance between two n-dimensional vectors x and y can be computed using Euclidean distance $\delta_{\ell_2}(x, y)$, and Manhattan Distance $\delta_{\ell_1}(x, y)$ metrics.

$$\delta_{\ell_1}(x, y) = |x - y| \tag{1}$$

$$\delta_{\ell_2}(x, y) = \|x - y\|^2 \tag{2}$$

3. Proposed Multimodal Biometric System

In the proposed approach, the multimodal system is implemented at the score level. A single trait from an individual is used with PCA, LBP and DWT algorithms to create three different unimodal versions of the biometric system. We have used the same classifier with the same score normalization algorithm to avoid some of the problems resulting from a different classifier score distribution and to bring the scores distributions from different feature extractors into a uniform distribution pattern before applying the proposed fusion techniques. In this way, an avenue is created for fair participation and contribution in the fusion process for all the unimodal systems.

3.1 Creating multimodal system

In our proposed method, we have created the multimodal biometric representation of an individual from a single trait (face data) but using different feature extraction algorithms (PCA, LBP and DWT). Since each feature extractor is different in its way of extracting feature, subsequently, each presented evidence is unique and differs from one another and hence gives a different unimodal system. As can be seen in Figure 4, the input biometric trait (face data) is used for creating the first unimodal representation by employing PCA algorithm to extract features. The second unimodal system is obtained with LBP. In the third unimodal system, initially DWT algorithm is applied to the face

image input to obtain four oriented wavelets from the decomposition process. The four oriented wavelets are concatenated together to form a single Joined Feature Vector (JFV). Subsequently, PCA is applied to the JFV to extract Reduced JFV (RJFV) which is shorter in size and contains more robust features than JFV alone. Figure 4 depicts how these unimodal systems are created for a given face image input named I.
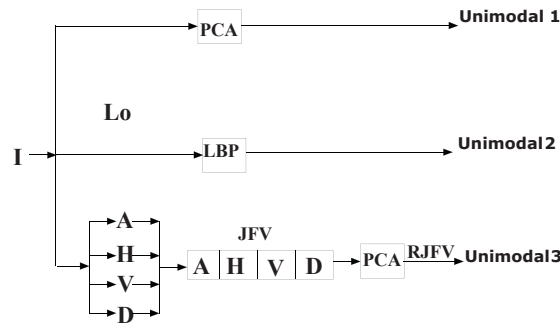
Figure 4. Unimodal feature extractions

3.2 Score normalization

The scores obtained from different unimodal systems have different statistical distributions and ranges since they belong to different sources. For making the distributions and the range similar so that each unimodal can contribute fairly in the fusion process, normalization becomes pertinent. Out of the many normalization schemes that exist, Min-Max (Eq. (3)) normalization is often suitable where the maximum and minimum bounds of the score produced by the matcher are known and hence it is adopted here [29-32].

$$S'_k = \frac{S_k - min}{max - min} \tag{3}$$

where S'_k is the normalised score, S_k is the original score and *min* and *max* are the minimum and maximum values of the scores distribution respectively.

3.3 Manhattan weighting penalty fusion

The MDPW is a new approach we propose to punish or penalize vector score in the training data (during test run) that have its scores away from the supposedly winning class which is a class with minimum Euclidean distance to the test data. Here the penalty is weighted, meaning that it is not the same for all vectors, and it linearly depends on how far is the vector from the winning class; the further the distance the more severe is the penalty while the closer the distance the more lenient the penalty. This penalty distance is added to each vector to put it further away from the supposed winning class based on its weighted penalty. Eq. (4) describes how this penalty weights are computed using Manhattan distance metric. For a given winning vector score x_w and score from some non-winning neighbors x_{nw}, the Manhattan penalty
(x_{mp-nw}) of x_{nw} can be computed using Eq. (4).

$$x_{mp-nw} = x_{nw} + \alpha|x_w - x_{nw}| \tag{4}$$

Where α is an integer constant and | | is the Manhattan operator or l_1-norm. Hence the new score is given as in the equation above. For *n* unimodal system the proposed fusion rule is given as the sum of the corresponding scores in each unimodal system.

Figure 5 depicts how scores are penalized based on their proximity or otherwise from the winning score. The score encircled in green indicates the winning class, and the rest are the non-winning classes. The red plots at the bottom of the figure denote the initial score distribution while the blue ones show the new scores after Manhattan penalty weighting.
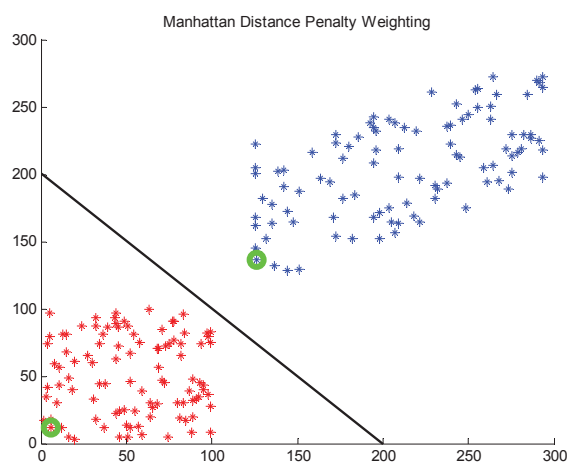
Figure 5. Manhattan penalty weighting scattered plot

4. Experimental Results

In this paper, two (ORL and YALE) databases are used to evaluate the performance of the proposed approach. The performance metrics that were used include; the percentage of Recognition Rate, False Accept Rate (FAR), False Reject Rate (FRR), and Receiver Operating Characteristics curve (ROC). To ensure adequate training and fidelity on the results obtained from the experiments; both training sets and testing sets were picked randomly from the database and each experiment was repeated ten times. In the end, an average of the performance of the ten runs is given as the system performance.

4.1 Simulation results using ORL database

The ORL database consists of 400 images acquired from 40 persons taken over a period of two years with variations in facial expression and facial details. All images are taken with a dark background, and the subjects are in an upright frontal position with tilting and rotation tolerance up to 20 degrees and tolerance of up to about 10% scale. All images are gray-scale with a 92×112 pixels resolution. The experiment is set up using the proposed fusion technique with the ORL database. The database is randomly divided into two equal parts; five samples from each subject in both training sets (200 images) and testing set (200 images) are used. The simulations are conducted in phases: (a) with three unimodal biometric setups with PCA, LBP and DWT alone and (b) with a multimodal biometric set formed from the four possible combinations of the PCA, LBP and DWT feature extractors. Each experiment is repeated ten times; each time randomly drawing training and testing sets from the database. The recognition rate for each set was recorded and presented in Table 1.

During the testing stage of the algorithm, each test image from the 200 images of the testing set makes a total of 5 genuine claims and 195 imposter claims from the training set. In total, 200 test images generate 5×200 (1,000) genuine claims and 195×200 (39,000) imposter claims. All the 1000 genuine claims and 2000 imposter claims are used for computing the FAR, FRR and ROC of the algorithm for performance evaluation. Figure 6 shows the comparison in ROC performance curve of all the system. Figure 7(a-c) show the plot of genuine and imposter score distributions of the three unimodal systems. On the other hand, Figure 8(a-d) show genuine and imposter scores of the four possible combinations of the multimodal system that are derived from the three unimodal systems.

Table 1. Comparison of the Recognition rates on ORL Database between the proposed fusion and others

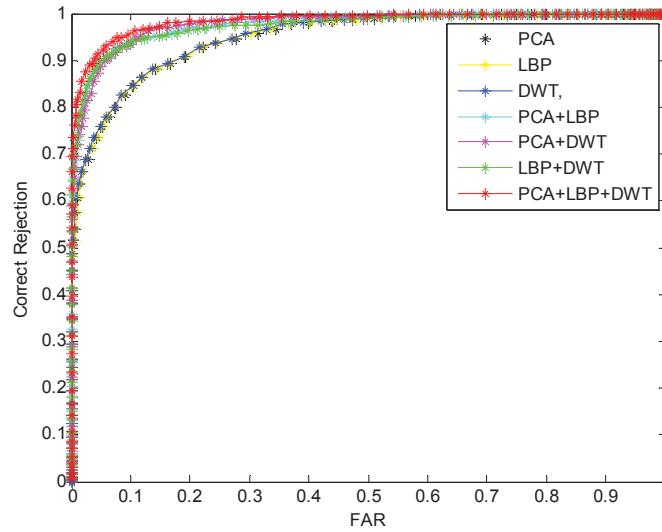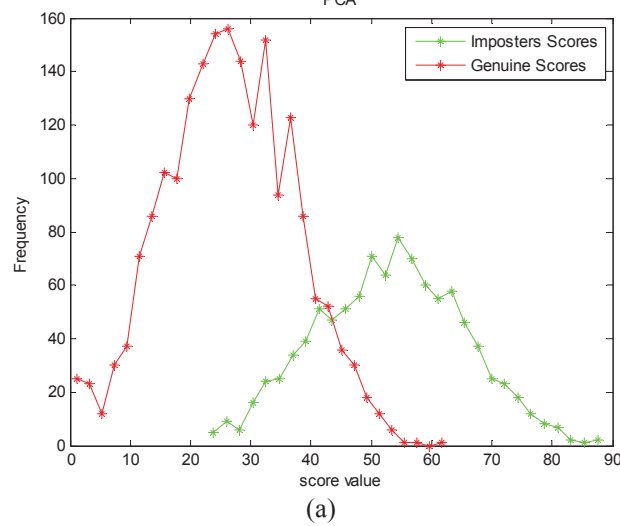| Fusion	PCA	LBP	DWT	1+2	1+3	2+3	1+2+3
Proposed	94.50	94.1	93.55	96.55	96.15	96.6	97.05
Sum rule	94.70	93.35	93.10	95.85	95.95	95.60	96.65
Product rule	94.9	94.5	94.05	94.20	94.00	93.85	91.65

Figure 6. ROC performance for the systems using the proposed approach

(a)

(b)

(c)
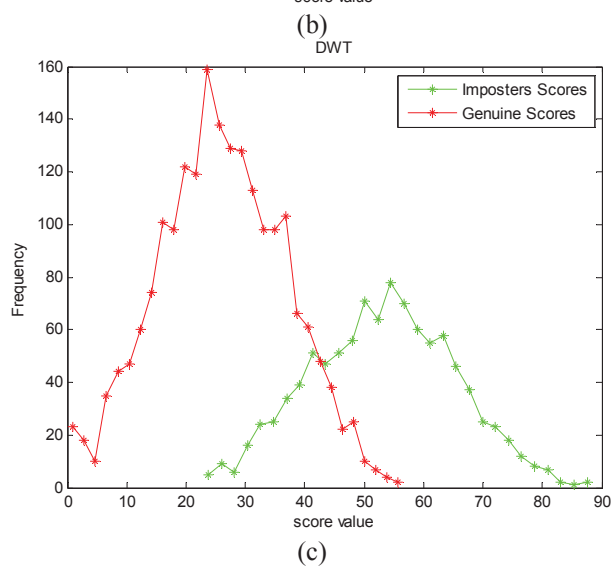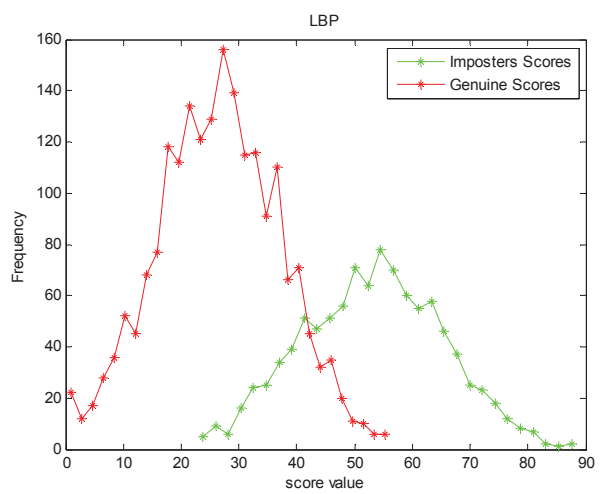
Figure 7 (a-c). Genuine and Imposter score distributions of the three unimodal systems based on the proposed approach

(a)
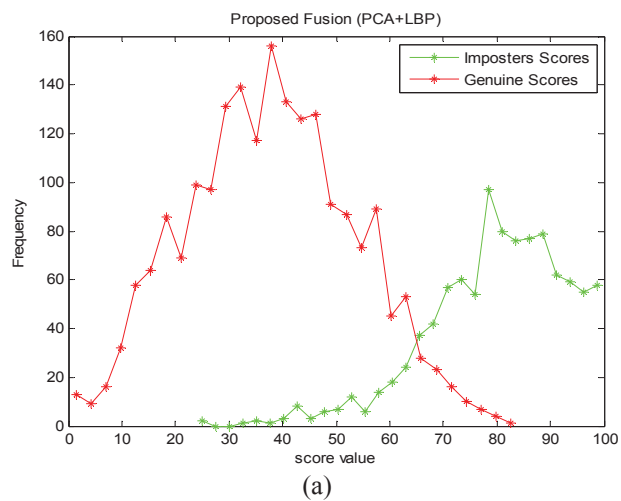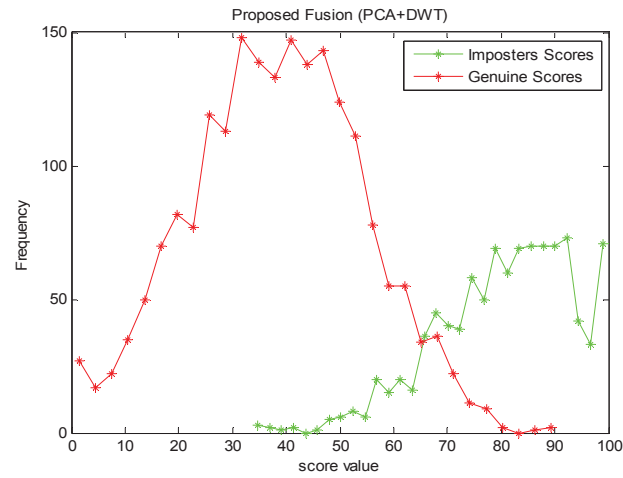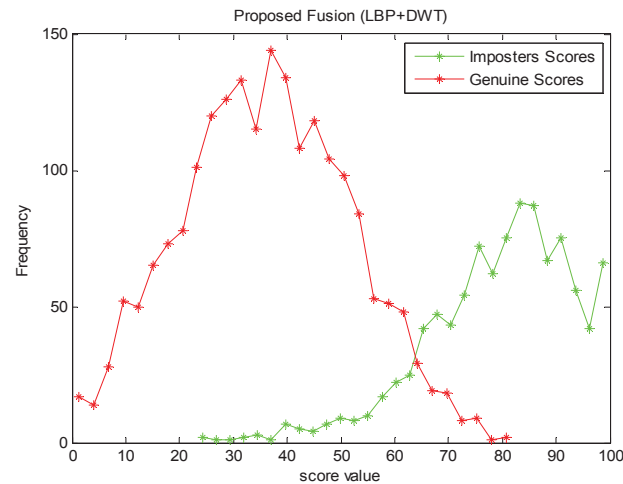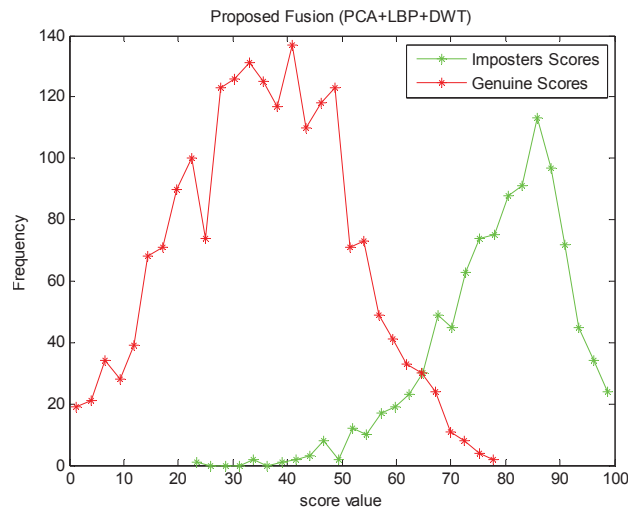
Figure 8 (a-d). Genuine and imposter score distribution of the multimodal system using the proposed approach

4.2 Simulation results using YALE database

Yale database contains 165 gray-scale images in GIF format belonging to 15 individuals. There are 11 images per subject, one per different facial expression or configuration: center-light, wearing glasses, happy, left-light, not wearing glasses, normal, right-light, sad as well as sleepy, surprised, and winking. The database is more complicated than the ORL and usually is used for facial expression recognition [33]. The same training procedures are adopted as in ORL and recognition rates of the proposed approach are compared with the other fusion rules available in the literature for performance comparison. Table 2 presents a comparison of the results obtained using the proposed method and other state-of-the-art fusion methods. Figure 10 depicts the similar results in a bar chart.

Table 2. Comparison of the recognition rates on YALE Database between the proposed fusion and others

Fusion	PCA	LBP	DWT	1+2	1+3	2+3	1+2+3
Proposed	69.06	73.73	70.80	75.33	73.80	77.73	83.60
Sum rule	68.40	74.27	71.20	75.33	72.80	76.13	79.20
Product rule	71.20	71.20	63.80	70.00	66.67	68.80	61.47
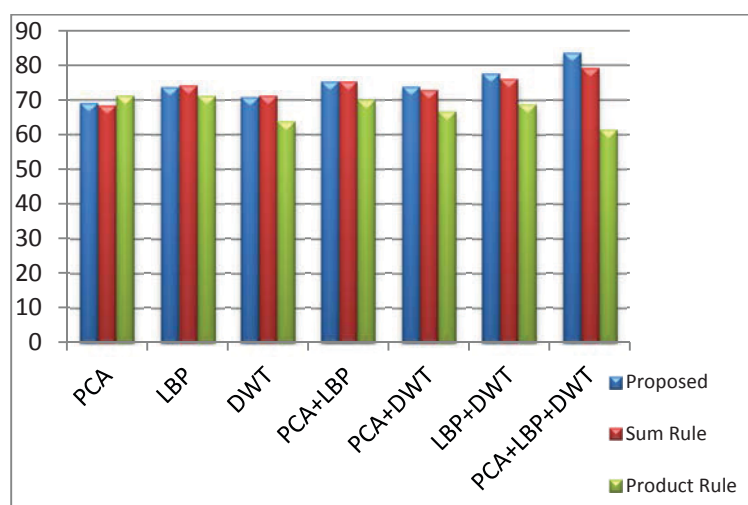
Figure 10. Bar chart of the recognition rate comparison on YALE database

5. Discussions

It is obvious from the experimental results that the proposed fusion rule based on Manhattan penalty weighting outperformed its counterparts (i.e. product and sum fusion rule). It is noteworthy that almost all the multimodal systems have better performance than the unimodal system in terms of recognition rates, FAR, FRR and ROC characteristics. The FAR and FRR curve performance of the proposed system has the list overlap (Figure 9(a)-(d)), which makes it a much more desirable system for both public convenience and high security applications. This property is more important than the overall recognition rate of the system in many access control applications. Moreover, it can be seen that fusion of more than two unimodal systems do not necessarily perform better than two unimodal systems as indicated by the experimental results. This trend may be traced to the fact that some models may have a very robust representation and other less robust, which overall may affect the fusion process.

6. Conclusion

A new approach for data fusion in the multimodal biometric system is proposed and implemented. Two face databases and data fusion techniques are used for implementing and comparing the obtained results with the proposed approach. Using ORL as a database, the experimental results show that the multimodal system has better performance than the unimodal system using PCA, LBP or DWT alone. Furthermore, results indicate that the proposed data fusion approach using Manhattan penalty weighting outperforms both of the two fusion techniques that use sum and product. This better performance concerns the recognition rate, FAR, FRR and EER of the algorithm. Similarly, in YALE database, the proposed approach has a lead in all the performance indices that are used for evaluating the algorithm performance. It is, however, noteworthy that the recognition rate in YALE database is not as good as that in ORL database. This is because there are so many variations within samples of the same subject which make it difficult for all algorithms to make a good generalization. Regarding the recognition rate, the proposed method has always had a better receiver operating characteristic which makes it much more suitable for many applications. In general, the new proposed fusion technique is promising and effective based on the experimental results. It performs better than its counterparts that were used in the literature.

References

[1] Belhumeur, P., et al., 1997. Eigenfaces versus fisherfaces: recognition using class specific linear projection, IEEE Trans. Pattern Analysis and Machine Intelligence, vol. 19, no. 7, pp. 711-720.

[2] Beyreuther, M., 2011. Speech recognition based automatic earthquake detection and classification, Ludwig Maximilians University, Muenchen, Fakultaet fuer Geowissenschaften, Ph.D. thesis.

[3] Bowyer, K.W., et al., 2006. Face recognition using 2-D, 3-D, and infrared: is multimodal better than multisample ?, Proceedings of the IEEE, vol. 94, no. 11, pp. 2000-2012.

[4] Bromba, M.U.A., Bioidentification frequently asked questions, available at http://www.bromba.com/faq/biofaqe.htm#ROC.

[5] Campbell, J., 1997. Speaker recognition: a tutorial, Proceedings of IEEE, 85, 9, pp. 1437-1462.

[6] CASIA iris image database, 2006. http://www.sinobiometrics.com .

[7] Chellappa, R., et al., 1995. Human and machine recognition of faces: a survey. Proceedings of the IEEE, 83, 5, pp. 705-740.

[8] Ross, A., et al., 2006. Handbook of Multibiometrics, SpringerScience + Business Media, LLC.

[9] Ratha, N.K., et al., 1998. Image mosaicing for rolled fingerprint construction. Proc. Int. Conf. Pattern Recog., vol. 2, pp. 1651–1653.

[10] Singh, S., et al., 2004. Infrared and visible image fusion for face recognition. SPIE Defense and Security Symposium, pp.585-596.

[11] Heo, J. Kong, et al., 2004. Fusion of visual and thermal signatures with eyeglass removal for robust face recognition. Proc. Joint IEEE Workshop Object Tracking and Classification beyond the Visible Spectrum.

[12] Son, B., and Lee, Y., 2005. Biometric authentication system using reduced Joint feature vector of iris and face. Lecture Notes in Computer Science, vol. 3546, pp. 261-273.

[13] Ross A., and Govindarajan, R., 2005. Feature level fusion using hand and face biometrics. Proc. SPIE Conf. Biometric Technology for Human Identification II, pp. 196–204.

[14] Kittler, J., et al., 1998. On combining classifiers. IEEE Trans. on Pattern Analysis and Machine Intelligence, vol. 20, no. 3, pp. 226–239.

[15] Verlinde, P. and Cholet, G., 1999. Comparing decision fusion paradigms using k-NN based classifiers, decision trees and logistic regression in a multi-modal identity verification application. Proc. Int. Conf. Audio and Video-Based Biometric Person Authentication.

[16] (AVBPA), 1999. Washington, DC, pp. 188–193.

[17] Chen, X., et al., 2005. IR and visible light face recognition. Computer Vision and Image Understanding, vol. 99. no. 3, pp. 332–358.

[18] Das, R., 2007. Signature Recognition. Keesing Journal of Documents & Identity, issue 24.

[19] Dass, S.C., et al., 2005. A principled approach to score level fusion in multimodal biometric systems. In Fifth AVBPA, Rye Brook, pp. 1049–1058, July.

[20] Daugman, J.G., 2004. How iris recognition works. IEEE Trans. Circuits Syst. Video Technol., vol. 14, no. 1, pp. 21–30.

[21]   Frischholz, R.W., et al., 1994. Face recognition with the synergetic computer. Proc. Int'l Conf. Applied Synergetics and Synergetic Eng., Fraunhofer Gesellschaft für Integrierte Schaltungen, Erlangen, Germany, pp. 107-11.

[22]   A. M. Ashir and A. Eleyan, 2015. A multi-resolution Approach for Edge Detection using Ant Colony Optimization. *23nd IEEE International Conference on Signal Processing and Communications Applications (SIU),* Malatya, Turkey, pp. 1777 – 1780.

[23]   Hampel, F.R., et al., 1986. Robust Statistics: The Approach Based on Influence Functions. New York: Wiley.

[24]   Han, J., and Bhanu, B., 2005. "Gait recognition by combining classifiers based on environmental contexts", Lecture Notes in Computer Science, vol. 3546/2005, pp. 113-124.

[25]   Ho, T.K., et al., 1994. Decision combination in multiple classifier systems. IEEE Trans. Pattern Analysis and Machine Intelligence, vol. 16, no. 1, pp. 66-75.

[26]   Huber, P.J., 1981. Robust Statistics. New York: Wiley. 21. Human identification at a distance. http://www.equinoxsensors.com/products/HID.html.

[27]   Indovina, M., et al., 2003. Multimodal biometric authentication methods: A COTS approach. Proc. MMUA 2003, Workshop Multimodal User Authentication, pp. 99-106.

[28]   ISO/IEC 24745:2011, 2011. Information technology - Security techniques – biometric information protection.

[29]   ISO/IEC TR 24722:2007, 2007. Information technology– Biometrics: Multimodal and other multibiometric fusion.

[30]   Jain A., et al. 2005. Score normalization in multimodal biometric systems. Pattern Recognition, vol. 38, no. 12, pp. 2270–228.

[31]   Jain, A., et al., 1999. A multimodal biometric system using fingerprint, face and speech. Second Internat. Conf. on AVBPA, Washington, DC, USA. pp. 182-187.

[32]   Jain, A., et al., 1997. On-line fingerprint verification. IEEE Trans. Pattern Anal. and Machine Intell., 19, 4, pp. 302-314.

[33]   Jain, A.K., and Ross, A., 2002. Fingerprint mosaicking. Proc. Int'l Conf Acoustic Speech and Signal Processing, vol. 4, pp. 4064-4067.

Implementation and Evaluation of Maximum Power Point Tracking (MPPT) Based on Adaptive Neuro-Fuzzy Inference System for Photovoltaic PV System

Abd El Hakim Ali Elagori*[1], M. Emin Tacer [2]

Abstract – The conversion of energy of sunlight into electricity is done using photovoltaic (PV) cells. This paper introduces, comparing, analyzing and evaluating the performance of the PV systems which are operating with MPPTs that work by adaptive neuro fuzzy interference system (ANFIS) technique with other MPPT algorithms such as Perturb and Observe (P&O) algorithm, Fuzzy Logic Control (FLC) algorithm and Artificial Neural Network (ANN) algorithm. These algorithms work to control the duty cycle (D) of the pulse signal that goes to the switch of the DC-DC converter for maximizing the power generated by the solar panel. The paper also introduces simulating and modeling a general PV panel with some adjustable parameters for modelling any real PV model using its electrical data sheet. In addition, the work tests the model for the influence of changing in operation solar irradiation and operation temperature on I-V and P-V curves. MPPT algorithms are implemented using boost DC-DC converter with constant resistive load. All systems are analyzed and simulated by using MATLAB-Simulink program. Simulation results show that the ANFIS and ANN based MPPT method gives faster response to archive the MPP and is more efficient than FLC MPPT and the P&O MPPT methods**.**

Keywords – *Photovoltaic cell, maximum power point tracking, fuzzy logic control, artificial neural network, adaptive neuro-fuzzy inference system*

1. Introduction

Renewable energy systems such as wind, sea waves and solar energy systems has been improving rapidly over the last few years and robust studies are maintained in this respect by researchers. Nowadays, solar energy is considered as one of the most reliable, daily available, free and environment friendly source of renewable energy when compared to other traditional energy sources such as coal, gas and nuclear oil which have negative effects on the environment that result in climate change [1,2]. Solar energy is one of the most common renewable energy sources that has been gaining increased world interest in recent years [3,4]. The conversion of solar radiation power to electrical power is done by a semiconductor device that is called Photovoltaic (PV) and the device produces electricity with direct electricity generation method. However, PV source is a non-linear source and the conversion efficiency is between 10% to 25% of the total power, moreover it is effected by the operation temperature (C°) and solar radiation (Kw/m²) [5]. Therefore, for maximum operating efficiency, it is necessary to use a maximum power point tracking (MPPT) algorithm to deliver possible available PV output power to the load at different operating points. MPPT is a power electronic device that contains DC-to-`-DC converter that includes controller work and one of MPPT algorithms. As seen in literature, various MPPT algorithms have been developed and many studies have been carried out to optimize these various MPPT techniques [6, 7].

With this technique, the system will force the PV cells to operate at its maximum power point (MPP). A MPPT such as the widely used Perturb and Observe algorithm (P&O) which is a conventional algorithm that tracks the MPP with constant step of duty cycle. The time response to reach the MPP depends on the value of the duty cycle; if the

[1]Corresponding author. Address: Department of Electrical Electronics Engineering, Engineering Faculty, Istanbul Aydin University, Istanbul, Turkey. Email: alagorei89@gmail.com, abdelhakimabobakirel@stu.aydin.edu.tr

[2] Dean of Electrical Electronics Engineering Department, Engineering Faculty, Istanbul Aydin University, Istanbul, Turkey. Email: emintacer@aydin.edu.tr

cycle is too small the time response will be large and vice versa. With intelligent control systems such as Fuzzy Logic Control (FLC), Artificial Neural Network (ANN) and the hybrid of the two of them as ANFIS, the performance of the system can be better than the conventional algorithm. ANFIS is an intelligent technique that can be used as intelligent maximum power point tracking control algorithms to optimize the performance of the PV system over the widest range of operating conditions.

The previous MPPT algorithms and ANFIS technique are used in this study for controlling duty cycle of the electronic switch of DC-DC boost converter. The PV system was operated under variable operation conditions to deliver the maximum power to the resistive load. All the simulations are done using MATLAB SIMULINK computer software.

2. Photovoltaic Cell

Electrical energy can be obtained directly from sunlight using photovoltaic (PV) devices (cells). The photovoltaic cells convert solar radiation power to electrical power under the photovoltaic effect [8, 9]. Photovoltaic (PV) cells are made from semiconductor materials. Usually the amount of the current for one cell is given in (mA) and the voltage is around 0.6 V. Cells are connected in serias and parallel to obtain the desired voltage and power [3].

2.1. Equivalent circuit of PV cell

The equivalent circuit of a solar cell can be categorized as p-n semiconductor junction, when exposed by the light, the DC current is generated in the terminal of the cell [10]. The equivalent electrical circuit which can represent the complex physics of a PV cell, is shown in Figure 1.
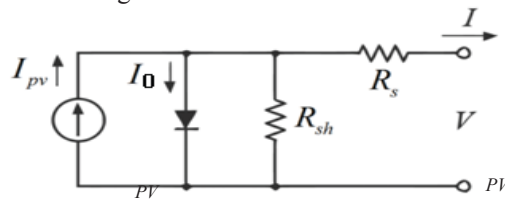
Figure 1. Equivalent circuit of PV cell

Output current characteristic is expressed with the following equations:

$$I_{pv} = I_{ph} - I^0 * \left[e^{\left(\frac{V_{pv} + I_{pv} * R_S}{A * K * T_{ak}} \right)} - 1 \right] - \left(\frac{V_{pv} + I_{pv} * R_S}{R_{sh}} \right) \tag{1}$$

$$I_{ph} = I_{scr} + K_i * (T_{ak} - T_{rk}) * G \tag{2}$$

$$I_0 = I_{rs} * \left(\frac{T_{ak}}{T_{rk}} \right)^3 * e^{\left[\left(\frac{q * Eg}{A * k} \right) * \left(\frac{1}{T_{ak}} - \frac{1}{T_{rk}} \right) \right]} \tag{3}$$

And for the large arrays modeling of Ns X Np series and parallel cells the equation becomes:

$$I_{pv} = I_{ph} * N_p - I_0 * N_p * \left(e^{\left(\frac{q(V_{pv} + I_{pv} * R_S)}{N_s * K * A * T_{ak} *} - 1 \right)} \right) - \frac{V_{pv} \frac{N_s}{N_p} + I_{pv} * R_S}{R_p} \tag{4}$$

where:

T_{rk}: The reference temperature = 298 K.
I_{ph}: The light generated current (A).
A: Ideality factor = 1.6.
q: Electron charge = 1.6×10^{-19} C.

I_{scr}:   The PV module short-circuit current.

K_i: The short-circuit current temperature Coefficient.

E_g: The band gap for silicon = 1.1 eV.

V_{pv}:   The open-circuit voltage or the output voltage (V).

I_{pv}:   The output current of the PV module (A).

I_{rs}:   The reverse saturation current (A) at T_{rk}.

k: Boltzmann constant = 1.3805×10^{-23} J/K.

R_s: The series resistance of the PV module.

R_p: The parallel resistance of PV module.

G: The PV module illumination (W/m^2).

N_s: The number of cells connected in series.

N_p: The number of cells connected in parallel.

I_o: The PV module saturation current.

T_{ak}:   Ambient temperature.

The relationship between the Current–Voltage and the Power-Voltage is used for describing the electrical characteristics of the PV cell and it is depicted as curve. The I-V and P-V curves of the PV cell has the shape shown in Figure 2, and power is obtained for a given radiation level [2].
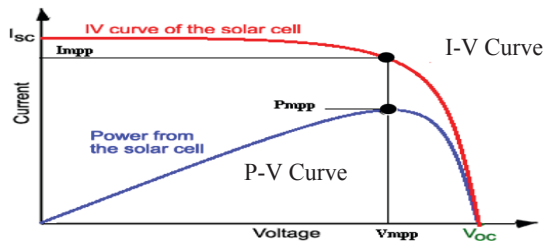
Figure 2. Power curves and maximum power point (MPP) of the PV cell

2.2 Temperature and solar radiation affection on PV output

Influence of changing on the operation solar radiation on the output power that when the amount of the radiation increases the short-circuit current (ISC) and open-circuit voltage (VOC) of the solar cell increase. As in the equation (2), the photon current is almost in a linear proportional relationship with irradiance. On the other hand, as the temperature increases, the open-circuit voltage decreases and the short-circuit current increases (Figure 3).
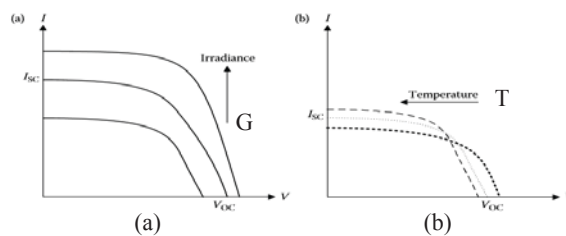
Figure 3. (a) Influence of the ambient irradiation and (b) Influence of the cell temperature on the cell I–V characteristics [3]

A general PV model is simulated in this paper using MATLAB Simulink to show the effects of varying temperature and solar radiation on the I-V and P-V curves. Scientists and researchers have been working to overcome these problems by adding intelligent power electronic systems connected to the PV system in order to force the PV system to run at its MPP.

3. Maximum Power Point Tracking

Maximum power point tracking (MPPT) is a technique used for maximizing power extraction from the available power in the PV module under all conditions. For maximizing the PV generated power, a DC-DC converter with MPPT algorithm is used by adjusting the duty cycle (D%) of the pulse signal that goes to the switch of the converter (Figure 4).
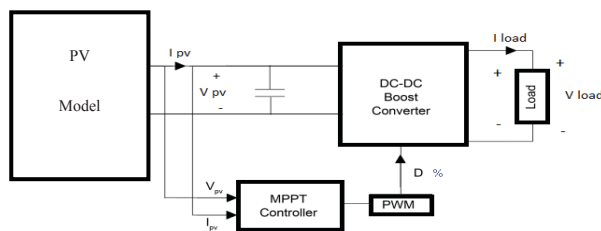
Figure 4. Black diagram of the MPPT with PV system

3.1 MPPT algorithms

The literatures are rich with many type of MPPT techniques based on different algorithms and with varying complexity. Many methods have been developed by researchers to determine MPPT [11, 12, 13,14]. The most popular MPPT method is P&O algorithm which is mostly used for evaluating the performance of the PV system compared to other MPPT algorithms [15]. The algorithms that will be presented in this paper are:

1. Perturb and Observe MPPT algorithm.
2. Fuzzy Logic control based MPPT algorithm.
3. Artificial Neural Network based MPPT algorithm.
4. Neuro Fuzzy interferons system based MPPT algorithm.

3.1.1. Perturb and observe method

The Perturb & Observe (P&O) technique is the most commonly used method of MPPT due to its ease of implementation and simple structures and it is highly competitive against other MPPT methods [13, 14, 16]. The main idea of this method is increasing the duty cycle with initial value (ΔD) mostly 0.01 and observing the power perturbation of the PV. If it is positive, then it runs in right direction and the operating point becomes closer to the MPP. As a result, new value is added to the current value of duty cycle in the same direction. And if the power perturbation of the PV is negative, that means the point of operation is moving away from the MPP. Therefore, the perturbation of the operating current should be reversed by the decrease in the duty cycle [17, 18].

Figure 5 presents the control flow chart of the P&O algorithm. The MPPT control system operates by incrementing or decrementing the solar array voltage periodically [19]. It measures the current and voltage of the PV at current iteration k and calculate P(k) as follows:

INTERNATIONAL JOURNAL OF ELECTRONICS, MECHANICAL AND MECHATRONICS ENGINEERING   *Abd El Hakim Ali Elagori, M. Emin Tacer*

Vol.7 Num.3 - 2016 (1453-1474)

Figure 5. The flowchart of the P&O Algorithm

One of the disadvantages of this algorithm is that the time response depends on the step size of the ΔD. if ΔD is a large value, the time response becomes fast to reach MPP but the operation point is not actually at MPP due to large perturbation [16].

In addition, if the step size of ΔD is a small value, the time response to reach MPP will be slow but the operation point can be very close to actual MPP with small perturbation; see Figure 6(a) which assumes the operation point at point1 where incising the duty cycle with positive ΔD voltage will increase and power the positive perturbation which wil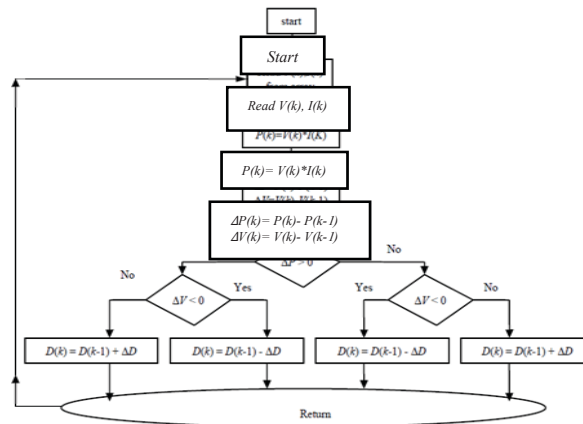l be at point 2, close to actual MPP, however, less than that. Therefore, the algorithm will increase the duty cycle with the same value of ΔD which in turn will increase the voltage but the operation will move away from the actual MPP at point 3, see Figure 6(b) where the perturbation will be negative then the next step will be back to point 4 and then to point 5 and from point 5 to point 6 and so on. This makes the operation point increasing and decreasing around the actual MPP; see Figure 6(c) where the cycle is reputed while the system is running [20, 21].
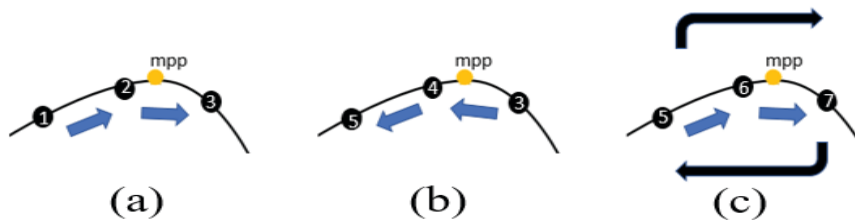
Figure 6. Perturbation of operation point (a) around actual MPP. Positive perturbation (b) Negative perturbation (c) Reputed cycle

3.1.2. *Fuzzy logic control based MPPT*

The Fuzzy Logic system was introduced by professor Lotfi A. Zadeh in 1965. Fuzzy logic is a form of logic used for expressing expert systems and has been applied in many fields from control theory to artificial intelligence applications. Fuzzy logic control system has faster and smoother response than conventional systems with a less control complexity [22]. Fuzzy logic includes a simple, rule-based IF X AND Y THEN Z approach for solving a control problem rather than attempting to model a system mathematically [21]. Fuzzy logic technique includes the following three steps:

1. **Fuzzification** – Convert classical data or crisp input into fuzzy data to Membership Functions (MFs) by using one of the fuzzy sets form mostly triangle fuzzy sets are used, see Figure 7.

2. **Fuzzy Inference Process** (Rule) – Combine membership functions with the control rules to derive the fuzzy output. This process is performed for determining a single MF among the group MFs by using operation on sets And, Or and Not this set has a membership degree. It is easy to build a rule base since it is closer to human languages; IF input high THEN output is low. Take air condition as an example; if it is hot than the fan is fast.

3. **Defuzzification –** After defining the set from rule base, the defined set or sets have membership degrees between 0 to 1 and by putting it in the output fuzzy sets that are defined from rules and by determining all the area under this degree (as seen in Figure 8, the MF degrees are a and b) after that will produce an area in one or two sets. These areas are fuzzy output as it is seen in Figure 8 and by calculating the centroid of the area or center of gravity that converts the fuzzy output to crisp output [23].

MPPT based fuzzy logic takes samples from the output of the PV system current (I) and voltage (V) at time (k) and calculate the result power P(k), with memories the measured previous sample at previous time (k-1) [26]. And it calculates the error E(k) and the change in error ΔE(k) :

$$P (k) = I (k) * V (k).\qquad\qquad(5)$$
$$P (k\text{-}1) = I (k\text{-}1) * V (k\text{-}1).\qquad\qquad(6)$$
$$\Delta P = P(k) - P(k\text{-}1).$$
$$\Delta V = V(k) - V(k\text{-}1).$$
$$E(k) = \frac{\Delta P}{\Delta V}\qquad\qquad(7)$$
$$\Delta E(k) = E(k) - E(k - 1)\qquad\qquad(8)$$

In the fuzzification process, the first step is the controller dose. This process converts the crisp input variables into linguistic variables using the membership functions. Five fuzzy sets with linguistic variable names of: NB (negative big), NS (negative small), ZE (zero), PS (positive small), and PB (positive big) as it is seen in Figure 7. The controller has two inputs and one output. The numeric variables are E(K) and ΔE(K) for inputs and D duty cycle for output. Each input has its membership functions and is same for the output. The value of a and b in the figure are selected by experience for acquiring the best performance [3, 17].
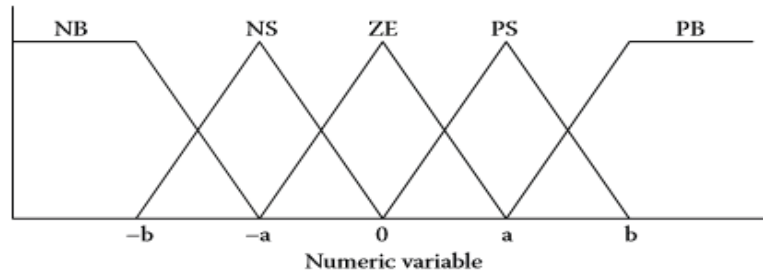
Figure 7. Membership function for inputs and outputs of MPPT based FLC

Fuzzy logic controller output diction is ΔD that will be added to current operation; D% increases and decreases with variable step size based on defuzzification process. The rules of the base system of fuzzy logic controller is presented in this table 1 [3].

Table 1. Rule base of fuzzy logic controller based MPPT in Table1

E(K) / ΔE(K)	PB	PS	ZE	NS	NB
PB	ZE	ZE	NB	NB	NB
PS	ZE	ZE	NS	NS	NS
ZE	ZE	ZE	ZE	ZE	ZE
NS	PS	PS	PS	ZE	ZE
NB	PB	PB	PB	ZE	ZE

As an example, for a certain control rule from Table 1, if Δ*E(K)* is *PB* and Δ*E(K)* is *NS* THEN *ΔD* is *NB*. This means that if the operating point is far from MPP towards right hand side and the change in *E(K)* is small, then the controller should decrease the duty ratio largely for reaching MPP. When both the Δ*E(K)* and *E(K)* are   changing by a small value, it means that the system is close to MPP so a small value will be added to the current D [3].

INTERNATIONAL JOURNAL OF ELECTRONICS, MECHANICAL AND MECHATRONICS ENGINEERING   *Abd El Hakim Ali Elagori, M. Emin Tacer*

Vol.7 Num.3 - 2016 (1453-1474)

3.1.3. Neural networks based MPPT

Another intelligent MPPT control technique is the neural network (NN). Artificial Neural Network (ANN) is an artificial network that mimics the human biological neural system. Networks behavior is widely used in modeling complex relationships between inputs and outputs in linear and nonlinear systems and used for data mapping and function approximation [24, 3].

The network structure of the three layers:

- Input layer: it contains the input features represented by nodes; each node is connected to every single node in the hidden layer and each connection has its weightiness that will be adjusted in the training process.

- Hidden layer: first it takes summation of the multiplication of each input node with connected weights than the output of hidden node is calculated by applying the activation function.
- Output layer: repeats the same process in the hidden layer to get the output. Figure 10 shows these layers.

The structural type of neural network that is used in this paper for building MPPT controller is multi-layer feed forward networks. The inputs of the MPPT controller in the input layer are generally two nodes PV set parameters, such as radiation (G), temperature (T) and one single output node in the output layer which represents the output decision (D). ANN processes these inputs, and determines the adapter operation duty cycle D% as the output resolution. The network must be trained off-line before being used in the system. Figure 8 shows a network that has three-layers where input layer **i** contains two nodes that represent the two inputs (*x1, x2*), the hidden layer **j** contains three nodes and one output layer, finally **y** contains one neuron connected to the previous neurons in the hidden layer [25].
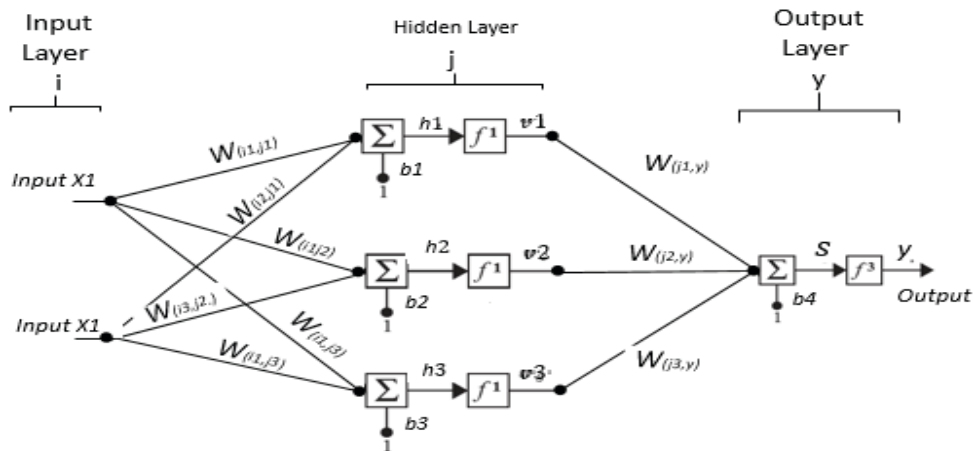
Figure 8. Three layers of multi-layer feed forward network structure

According to the figure above, the output of the network can be calculated by:

$$h_j = \sum (W_{(i,j)} * x_i + b) \tag{9}$$

where $W_{(i,j)}$: the weight of connections between input node **i** and the hidden neuron **j**.

b : Bias parameters like the weights usually have constant of 1.

The output of neurons in the hidden layer calculates vj by applying the activation function (*f*) sigmoid function is usually used as transfer function.

$$vj = f(hj) = \frac{1}{1-e^{-hj}} \tag{10}$$

The calculation of the hidden neurons' output multiplication summation according to neuron weight by; according to their weights by:

$$S_o = \sum \left(W_{(j,y)} * v_j \right) + b_4 \tag{11}$$

Then the output of the network y can be calculated by applying the activation function on s.

$$y = f\left[v_1 * W_{(j_1,y)} + v_2 * W_{(j_2,y)} + v_3 * W_{(j_1,y)} + b_4 \right] = f(s)$$

Where $W_{(j,y)}$ weights of the connection between the hidden layer neuron j and the output neuron y

f: Transfer function, usually the sigmoid function is used and it takes the form of:

$$y = f[s_0] = \frac{1}{1 - e^{-s_0}} \tag{12}$$

Throughout the training, the connection weights are modified until the best fit is attained for the input–output patterns from the training data set based on the minimum errors that are selected.

❖ *Backpropagation Learning Algorithm*

Any neural network must learn the tasks first before putting it in the system [25, 26]. The type of learning that is used here is supervised learning algorithm which makes the network learn from examples in the training data. The teach way is by setting and adjusting weights between nodes. The initial weights are usually set at random numbers and then they are adjusted during NN training. Supervisor Backpropagation learning algorithm is used for training the multilayer feed-forward network, it works to decrease the error between the desired and computed unit values. That by propagating the error from the output layer to the input layer. A new set of weights which minimizes the error, is also determined during this process. The general learning procedure in the backpropagation algorithm is achieved by following the steps and equations below:

1. Calculate the summation of the node in the hidden layer of the feed-forward ANNs in the figure using Eqn (9).
2. Apply activation function to get output of the hidden neuron using Eqn (10).
3. Calculate Summation of the node in the output layer by using Eqn (11).
4. Apply activation function to get output *y* of the output neuron by using Eqn (11).
5. Then compute the cost function which is the mean square error in the output.

$$E = \frac{1}{2} \sum (y^d - y)^2 \tag{13}$$

Where ^{d} : is the Desired Output, and y is the Calculated Output.
E: the mean square error in the output.

6. Update the old weight $W_{(j,y)}$ in iteration *t* by:

$$W_{(j,y)}(k+1) = W_{(j,y)}(k) + \int * \frac{\partial E}{\partial W_{(j,y)}} \tag{14}$$

Where $\int$: learning rate or correction factor constant effects on the step size of the minimizing the square error and it determines the speed of the learning, if it is small the network learns slow.

$W_{(i,j)}$: the weight between node i and node j.

INTERNATIONAL JOURNAL OF ELECTRONICS, MECHANICAL AND MECHATRONICS ENGINEERING   *Abd El Hakim Ali Elagori, M. Emin Tacer*

Vol.7 Num.3 - 2016 (1453-1474)

The calculation of the propagation error $(\frac{dE}{dWjy})$ between hidden and output layers is done by finding the derivative of the error with respect to the weights. Solving the partial derivatives of the error can be derived by the chain rule after solving equation (14)

$$W_{(j,y)}(k+1) = W_{(j,y)}(k+1) + \int * y * (1-y) * vj * - \quad (y^d - y) \tag{15}$$

Update the old weight $W_{(i,j)}$ in iteration k by:

$$W_{(i,j)}(k+1) = W_{(i,j)}(t) + \int * \frac{\partial E}{\partial W_{(i,j)}} \tag{16}$$

The calculation of the propagation error $(\frac{\partial E}{\partial W_{(i,j)}})$ is done by solving the partial derivatives of the error also by the chain rule. Finally find the new $W_{(i,j)}$ using equation:

$$W_{(i,j)}(k+1) = W_{(i,j)}(k) - \int * x_i * W_{(j,y)} * v_j * (1-v_j) * (y^d - y) * y(y^d - y) \tag{17}$$

These basic steps should be done for one sample from the training data. First, all weights are selected randomly and the minimum error that is allowable is determined then the network is fed forward to calculate the actual output and if the result is not the same with the desired output, that means the mean square error is bigger than the allowable error [26]. It can be said that the algorithm learns through iterations. The number of iterations in typical network can be any number from ten to ten thousand. Therefore, training it is hard to be done manually, even for the very small amount of training data, therefore for large training data computers are used to train the network. **MATLAB** program has neural network tools which make it easy to build the network and train it using any training data.

A neural network will be built and trained in this study using the data that contains all possible operation temperature and solar radiation as inputs, and their best decision of duty cycle as output to work as MPPT controller. The performance of the ANN based MPPT controller depends on how well the network is trained.

3.1.4. *Adaptive neuro-fuzzy inference system based MPPT*

Another MPPT algorithm uses an artificial intelligence technique which is proposed to be called ANFIS and is an efficient algorithm for working with MPPT concept; it has also been applied and proved its efficiency [27, 28]. The Fuzzy logic system is a useful tool for building a system based on human thinking without modelling the system mathematically. The output decision of FLC is based on the written rules to make defuzzification on the output membership functions parameters. These parameters are designed by an expert or by the experiences and adjusted several times in order to improve the performance of the controller. The artificial neural network system has capabilities of learning from examples or learning from data as it is seen in the previous section.

An adaptive neuro-fuzzy inference system or adaptive network-based fuzzy inference system has been introduced by Jang in [29] for constructing a fuzzy logic controller. ANFIS is a kind of artificial neural network that uses learning capabilities and hybrid learning of ANN to generate fuzzy IF-THEN rules and select the membership functions parameters of the Takagi–Sugeno fuzzy inference system, a set of input-output samples, from training data for mapping or approximating any nonlinear system. ANFIS architecture is shown in Figure 9 [30].
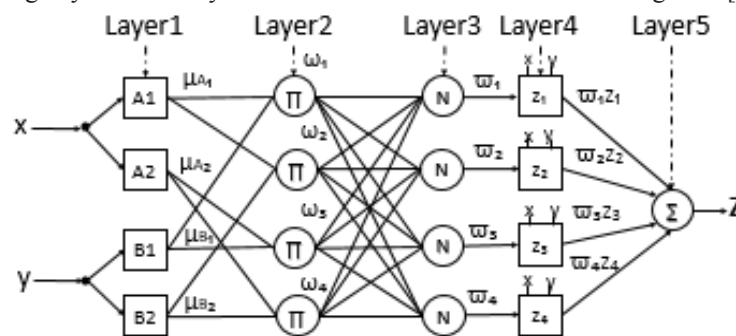

Figure 9. Architecture of ANFIS with four rules and two membership function for each input

ANFIS in Figure 12 has two inputs; x and y, and one output; z. For the first-order in Sugeno fuzzy model, a typical rule set with four fuzzy if-then rules can be expressed as:

Rule: If x is A and y is B, then z = (p*x+ q*y + r)

where Ai and Bi are the fuzzy sets in the antecedent, and p_i, q_i and r_i are parameters which are determined during the training process.

ANFIS consists of five layers, and the nodes in each layer depend on the number of inputs, membership function and rules and mostly on a single output as it is seen in Figure 9:

❖ **Layer 1:** this layer consists of the number of nodes, and *i* represents inputs membership functions.

$$\begin{cases} O_{(1,i)} = \mu A_{i(x)}, & i = 1,2 \\ \\ O_{(1,i)} = \mu B_{i(x)}, & i = 3,4 \end{cases}$$

(18)

where: μAi(x) and μBi(y) membership degrees can be obtained by the fuzzification process; for example Triangular membership function is mostly used with the equation below:

$$\text{Triangle}(x; a, b, c) = \begin{cases} 0 \quad, & x \le a \\ \frac{x-a}{b-a}, & 0 \le x \le b \\ \frac{c-x}{c-b}, & b \le x \le c \\ 0, & b \le x \le c \end{cases}$$

(19)

where {a,b,c} is the parameter set that change the shapes of the MFs, and the parameters in this layer are called premise parameters

❖ **Layer 2:** each node in this layer receives the linguistic variables with MF degrees and calculates the firing strength of a rule via multiplication and sends it to the next layer. T-norm operators can be used as AND function to rule the firing [18].

$$O_{(2,k)} = \omega_k = \mu A_{i(x)} \mu B_{J(x)}, \quad i=1,2, j=1,2; \quad k = 2(i-1) +j$$

(20)

Where *k:* represents the output number.

❖ **Layer 3:** The outputs are called normalized firing strengths that by calculate the ratio of firing strength rule in the *i* node that comes from previous node to the sum of all rule's firing strengths.

$$O_{(3,i)} = \overline{\omega}_i = \frac{\omega_i}{\omega_1+\omega_2+\omega_3+\omega_4} \quad ,i=1,2,3,4$$

(21)

❖ **Layer 4:** Output of each node in this layer has the following function:

$$O_{(4,i)} = \overline{\omega}_i z_i = \overline{\omega}_i(p_i x + q_i y + r_i) \quad ,i=1,2,3,4$$

(22)

Where $\overline{\omega i}$: is referred to as the normalized firing strength from layer 3

p_i, q_i and r_i: is the parameter set of *i*th node. These are referred to as consequent parameter

❖ **Layer 5:** The output node in this layer computes the overall output as the summation of all incoming signals divided summation of all weights or all rule's firing strengths from layer 2.
It can be expressed as:

$$O_5 = \frac{\omega_1 z_1 + \omega_2 z_2 + \omega_3 z_3 + \omega_4 z_4}{\omega_1 + \omega_2 + \omega_3 + \omega_4} = \sum_{i=4}^{4} \overline{\omega}_i \, z_i = \sum_{i=4}^{4} \overline{\omega}_i(p_i x + q_i y + r_i)$$

(23)

The structure of a neuro-fuzzy system is like a multi-layer neural network. The square nodes in Figure 9 have adjustable parameters and the circle nodes have fixed parameters. The basic learning algorithm to optimize ANFIS parameters are backpropagation gradient descant algorithm which has been used for training the multi-layer ANN (see section 3.1.3) [31]. During the learning process, in order to achieve a desired input-output mapping, the premise parameters (*a, b, c*) in the layer 2 and the consequent parameter (p_i, q_i, r_i) in the layer 4 are updated according to the given training data and are trained until the desired response in the output is achieved.

❖ *Basic ANFIS Learning Algorithm*

Firstly, the training data set should be available to feed the inputs in the ANFIS network that mostly has two inputs. Second thing is selecting the number of the fuzzy membership function for each input and defining the kind of functions. The triangular is selected in this paper which has parameter (a, b, c), see equation (19); these parameters are named premise parameters. The number of rules can be determined by the multiplication of the number of MF sets of the input1 with the number of MF sets in the input2. Then, it calculates the final output and total square error by:

$$E = \frac{1}{2}\sum(O^d - O_a)^2 \tag{24}$$

Where O^d : desired output.
O_a: actual output.

The general equation of backpropagation for updating both the premise and the consequent parameters is:

$$\alpha\ (k + 1) = \alpha\ (k) + \int * \frac{\partial E}{\partial \alpha} \tag{25}$$
Where ,∫: learning rate.
α ∶ is any updating wanted parameter.

The MATLAB program includes an ANFIS tool which is used for building the FLC controller utilizing the process of training the ANFIS, based on the training data that contains vector of the inputs representing the operation temperature and the operation solar irradiation and the vector that represents the best decision of duty cycle is given to the system to run at MPP. MPPT based ANFIS have been seen in the literatures [27, 32].

3.2. Boost Dc-Dc convertor

Dc-Dc converters are power electronic circuits that convert a dc voltage to a different dc voltage level. It basically consists of a voltage source, an inductor, a power electronic switch (usually a MOSFET or an IGBT) and a diode. It usually also has a filter capacitor to deliver the output voltage. Its function is to step up input DC voltage to bring it to a desired level in the output. Figure 10 shows functional circuit of a boost converter which operates by periodically opening and closing an electronic switch. It is called a boost converter because the output voltage is larger than the input [33].
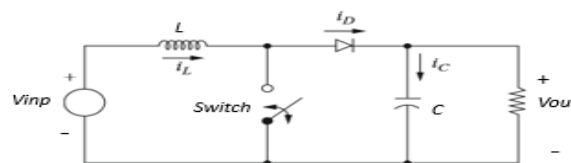
Figure 10. The boost converter circuit

The output voltage level is controlled by adjusting the ratio duty cycle (D%), on/off time of the switch. When the switch is in the **ON** state (closed), the diode is reverse biased and the whole circuit will be divided into two loops; one at the output side and another at the input side. Applying a dc voltage across an inductor   for a period (usually in the 20 kHz to 5 MHz range) which causes starts to charge the inductor. On the other hand, when the switch is in the **OFF** state (open), the diode becomes forward-biased and there will be a closed loop consisting of power source, inductor and RC load. The energy stored in the inductor during the **ON** state (closed switch) is discharged to the RC load circuit through the closed diode.

The relation between input and output voltage is given by this equation:

$$V_{out} = \frac{V_{inp}}{(1-D)} \tag{26}$$

Where D: DC-DC converter's duty cycle.

For designing the minimum inductance for continuous current in the boost converter is given by :
$$L_{min} = \frac{D*(1-D)^2*R}{2f} \tag{27}$$
Designing aboost converter for continuous-current operation will have an inductor value greater than: L_{min}.[22] and capacitor value is given by :

$$C_{min} = \frac{D*V_{out}}{R*\Delta V\%*f} \tag{28}$$

Where f: is the switching frequency. Alternatively, expressing the capacitance in terms of the output voltage ripple yields:

ΔV :Output voltage rippel.

For designing boos converter, usually C is selected greater than C mine.

The tracking efficiency of the MPPT algorithm is given by:

$$\eta\text{-MPPT} = \frac{P_{out}}{P_{mpp}-loss} \tag{29}$$

P_{mpp} is the possible (theoretical) achievable power.

Pout is the power extracted from the PV array by the MPPT algorithm that is used; it depends upon the ability of the MPPT to be as close as possible to the MPP [34]. η -MPPT is not concerned with the physical efficiency of the converter (for example, switching loss). The next chapter will implement all the MPPT algorithms presented in this chapter using MATLAB program and run each algorithm with PV system in Simulink environment for analyzing the performance of each case.

4. PV Model and Simulations of Case Studies

This section shows all the simulations of all the systems; the Photovoltaic PV model, boost converter and MPPT controller based on the purposed MPPT algorithms. All the simulations are done using MATLAB/SIMULINK software. This chapter discusses all the case studies and simulation results for the whole system. The next section contains modeling a general PV panel and shows some results regarding the effects of temperature and solar radiation on PV output power and MPP operation.

4.1 PV model simulation

Among the objectives of this paper are simulating a PV model and estimating the I-V characteristic curves of the PV under different operation temperature and solar irradiation and use this simulated model for testing the dynamic performance of MPPT later. The simulation is done by MATLAB Simulink which models the equations (1,2,3,4) using subsystem blocks for building a general system that can model any PV system that contains one or more than one model as array. The simulated equations of the subsystems are shortened in one block, as shown in Figure 11 (a) and as shown in Figure 11 (b) by using mask parameter property there are some parameters designed to be adjustable. In addition, the PV model in Figure 11 (a) contains temperature (T) and solar irradiance (G) input which will be used as adjustable values for testing and analyzing the performance of the PV model [35] . A PPS**130W AS8118** PV module characteristic data (Product abailable on Alibaba wibsid Solar Panel [250812]) which is shown in Table 2, was taken as the reference for simulation and analyzing temperature and solar irradiance affections on the output power.
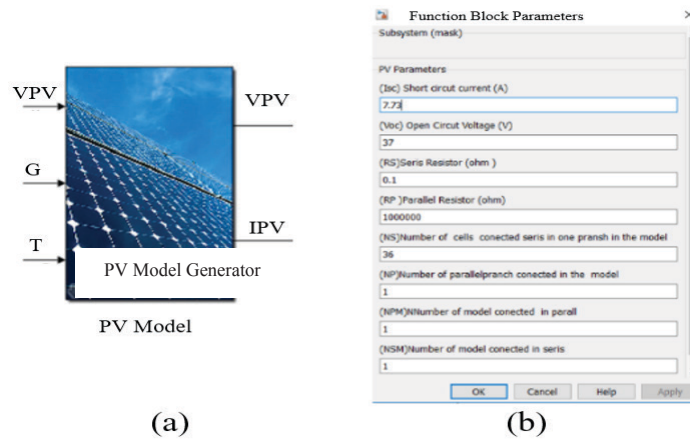
Figure 11. The main model of the PV (a) PV model block (b) Subsystem mask parameters

Table 2. Electrical Data of **PPS130W AS8118** PV Module

Electrical Data Under STC	Value
Maximum Power (Pmax)	130W
Maximum power voltage (Vmpp)	18V
Maximum Power current (Impp)	7.23A
Open Circuit Voltage (Voc)	22.5V
Number of Cells	36 pcs

The simulation model is tested by connecting the model with a variable resistor load which is controlled to start from short circuit to open circuit and then plotting the relationship between the current and the voltage which represent I-V curve as well as the power and the voltage which represent P-V. Figure 17 shows the simulation circuit. The first test was done by applying constant operation solar radiation 1000 kw/m² with a changing temperature from 5 C° to 35 C ° with step of   5 C°. On the other hand, the second simulation test was done by applying constant operation under the temperature of 25° with a changing solar radiation from 600 kw/m² to 1000 kw/m² and an increasing step of 100 kw/m². Figure 12 shows the simulation circuit.
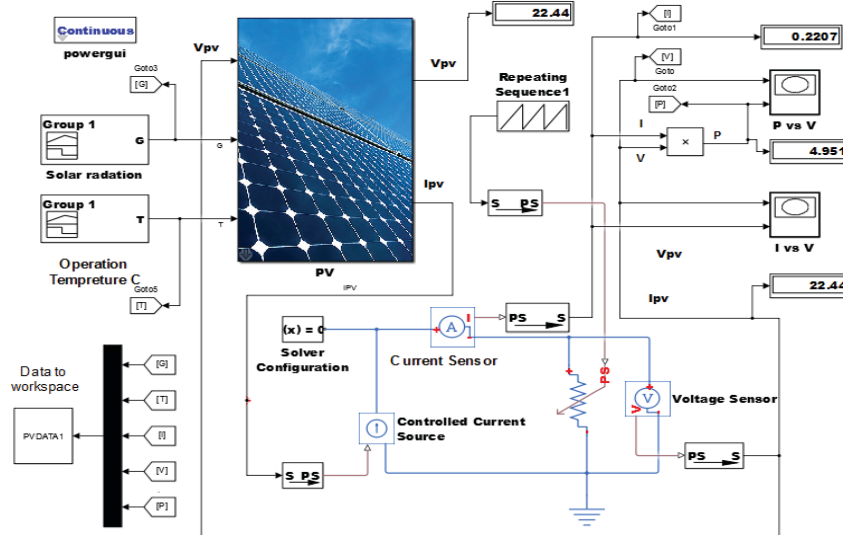

Figure 12. MATLAB simulation circuit for testing the PV simulation model

The result in Figure 13 (a) is seen in the plot. We have concluded that whenever the temperature increases the voltage and solar radiation, short operation current and the power output increase as well. The contrary happens with a small change in voltage. The power output decreases and vice versa, as seen in Figure 13 (b).
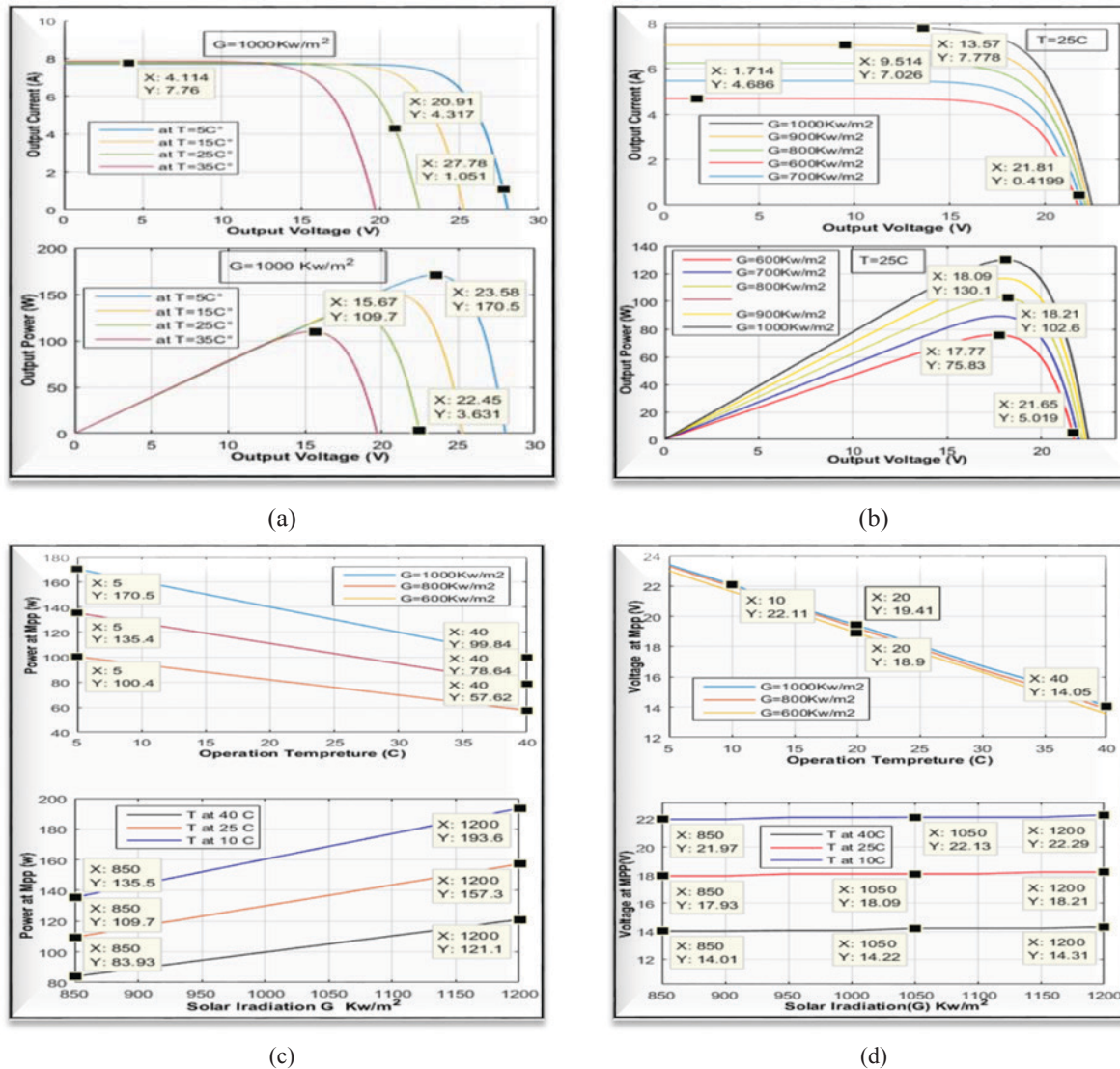

(a)

(b)

(c)

(d)

Figure 13. Influences of T and G (a), Influence of T on *V-I* and *P-V* curves (b), Influence of the G on *V-I* and *P-V* curve (c), Influence of G and T on MPP (d), Influence of G and tempreture on Vmpp

Regarding the result seen in Figure 13 (c), we have concluded that MPP operation increases when the radiation increases and the vice versa happens with the temperature increase. Figure 13 (d) shows how the VMPP increases when the temperature decreases and is approximately at constant when the radiation changes. These results prove that the operation point and maximum power point are the V-I curve and P-V curve and they are changing with any change in solar irradiation and temperature, according to the situation and the seasons of the year. A DC-DC convertor controlled with MPPT technique is used for maximizing the PV power and delivering it to the load. The next section shows the simulation circuit for boost DC-DC converter which is used for analyzing the performance of the proposed MPPM algorithm in this paper.

4.2. Boost convertor model simulation

The parameters for the DC-DC boost converter are shown in table 3. The switching frequency (fs) is selected as 200Kh and the inductor value (L1) was selected greater then L min in equation (3.6) and the capacitor values (C1, C2) were chosen in order to obtain a fast response for the MPPT algorithms. The simulation circuit of the convertor is shown in Figure 4.11**.**

Table 3**.** Boost DC-DC convertor simulation parameters

Parameter	Value
Inductance L1	1mH
Capacitor C1	1**μ**F
Capacitor C2	200**μ**F
Load resistor R	10**Ω**
Switching Frequency Fs	200kH

4.3 Perturb and observe MPPT controller

The first system contains the PV system and is controlled based on P&O MPPT method. P&O is implemented using MATLAB function and programed using MATLAB M-file based on the flowchart given in Figure 5. The initial value of ΔD is selected as 0.001 and the time sample of given decathlon is selected as 0.02 ms.

4.4 Fuzzy logic controller model

Fuzzy controller based MPPT is designed using MATLAB Fuzzy logic designer tool. The controller has two inputs; the first one represents the calculated input error E(k) value and the second input represents the delay of error E(k) and the single output represents the ΔD decision, last but not least the MFs were selected as shown in Figure 14 (a,b,c) below.
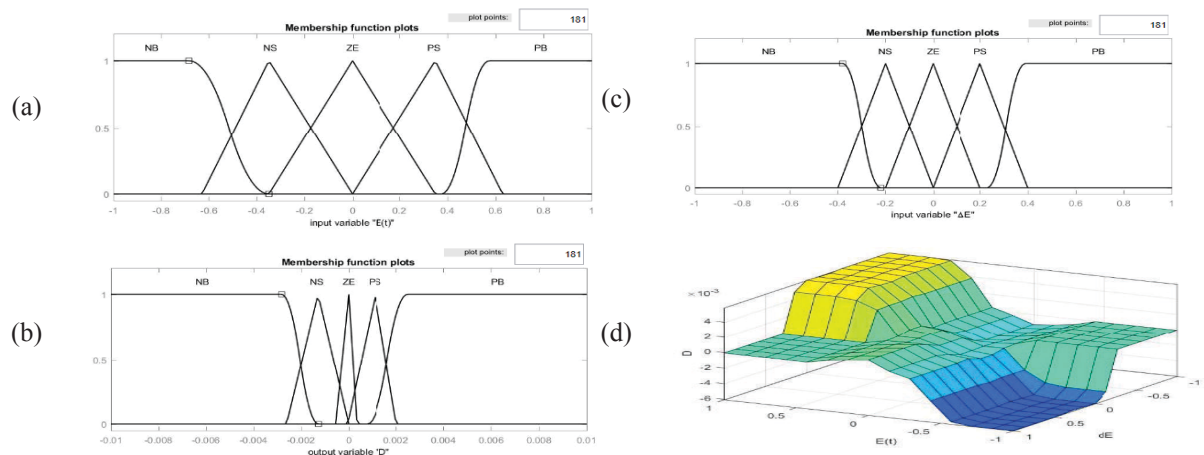

Figure 14. Membership functions of FLC based MPPT : (a) MFs of input error E(k) (b), MFs of input delta E(k) (c), MFs of output decition (c), Inference rule base surface of FLC based MPPT

The designed fuzzy logic controller shoud be imported to work space for use in simolink with the fuzzy contrloller block, where the controller can take samples of the calculated E(k) and E(k-1). The time sample of the given decision is selected as 0.08 ms for obtaining an efficient performance.

4.5 Neural Network Controller Model

The ANN controller based MPPT is designed using MATLAB M-file code [36] and trained using backpropagation learning algorithm with 126 training sample which is obtained by operating the two PV systems. The first one works with P&O MPPT and a smaller constant value, just to determine the range of the duty cycle. Later, copied to the second PV system that running with the adjustable duty cycle for increasing and decreasing the duty cycle for obtaining an accurate and reliable result. The ANN which is shown in Figure 15 (a), is designed with ten hidden layers, two inputs and one output.
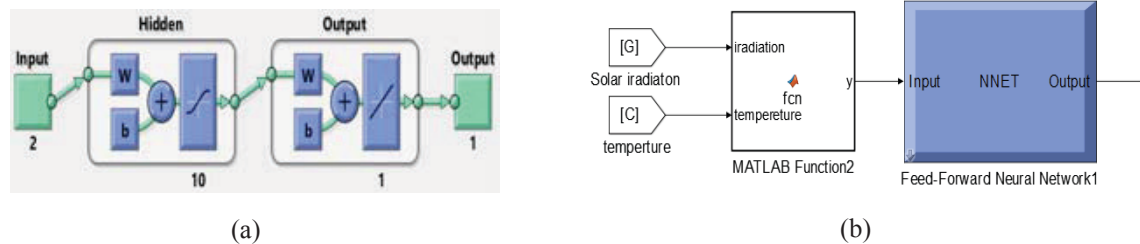

(a)   (b)

Figure 15. (a) Neural network stricture based MPPT, (b) Simulation circuit of ANN controller based MPPT

In Figure 15 (b), ANN controller has two inputs (solar irradiance and temperature) and one output which is the duty cycle that operates at maximum power point. The MATLAB function which is used for arranging the values of G and T as vectors, is located between the network and the inputs.

4.6 Neuro-Fuzzy controller model

MATLAB Neuro-Fuzzy designer tool is used for training the ANFIS with the same training data that the ANN controller is trained. Backpropagation training algorithm is used for optimizing the FLC parameters and generating the system, as shown in Figure 16 below.

Figure 16. The structure of the generated FLC system after the ANFIS training

MFs are selected for each input and their parameters are optimized during the training process. The output is the optimized MFs as constant samples during the training process.
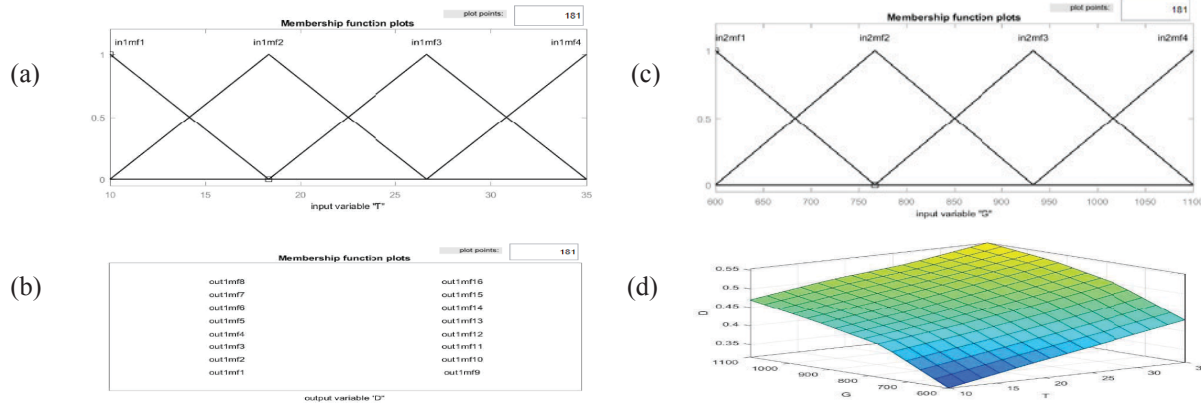
MFs membership functions are given below:

Figure 17. Generated membership functions (a), MFs of temperature (b), MFs of solar irradiation (c), Output samples of the Sugeno FLC system (d), Inference rule surface of FLC generated by ANFIS

The inference rule base is optimized during the ANFIS training process, as shown in Figure 17 (b) whereas the rule surface is demonstrated in Figure 17(c). The previous generated FLC should be imported in MATLAB work space in order to be used as a controller in Simulink environment.
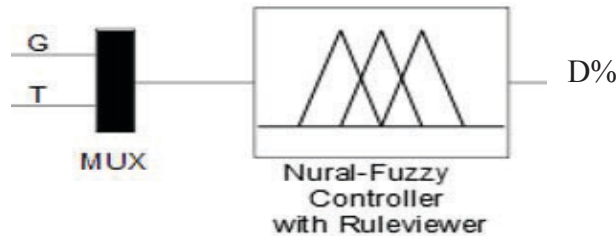

Figure 18. Purposed FLC controller based MPPT whose parameters are generated by ANFIS training

5.   Simulation Circuit of Proposed PV Systems

The complete system is simulated using the MATLAB/SIMULINK (See Figure 19) where each block in the simulation represents a kind of PV system. The simulation is done by operating the five PV systems where each system has the same PV model and boost converter parameters but a different MPPT mechanism.

For controlling the duty cycle with each system:

1) The first PV system which is shown in block 1 in Figure 23, operates without any controlling for tracking the MPP and the duty is selected as 0.503 to operate PV system at its MPP only case of solar irradiation equals 1000 Kw/m² with the temperate of 25 Cº. Note that D is constant and does not change depending on the variations in the values of G and T.
2) Second PV system which is shown in block 2 in the figure, works with MPPT of P&O algorithm for guiding the PV system to the possible MPP operation.
3) Third PV system which is shown in block 3 in the Figure, works with FLC controller based MPPT.
4) Fourth PV system which is shown in block 4 in the Figure, works with ANN controller based MPPT.
5) Fifth PV system which is shown in block 5 in the Figure, works with FLC controller that is designed by the ANFIS training based MPPT.

Each system will be running with variation in temperature and solar irradiation in order for the researchers to observe the effects on the output power of each system for analyzing the performance of each MPPT controller and thus see what happens to the output power of the PV system work without an MPPT controlling algorithm. The simulation result and the conclusion are presented in the next and the last section which offers a conclusion together with a comparison regarding the performances of all the PV systems summarizing how the performance of each PV system differs from one another.
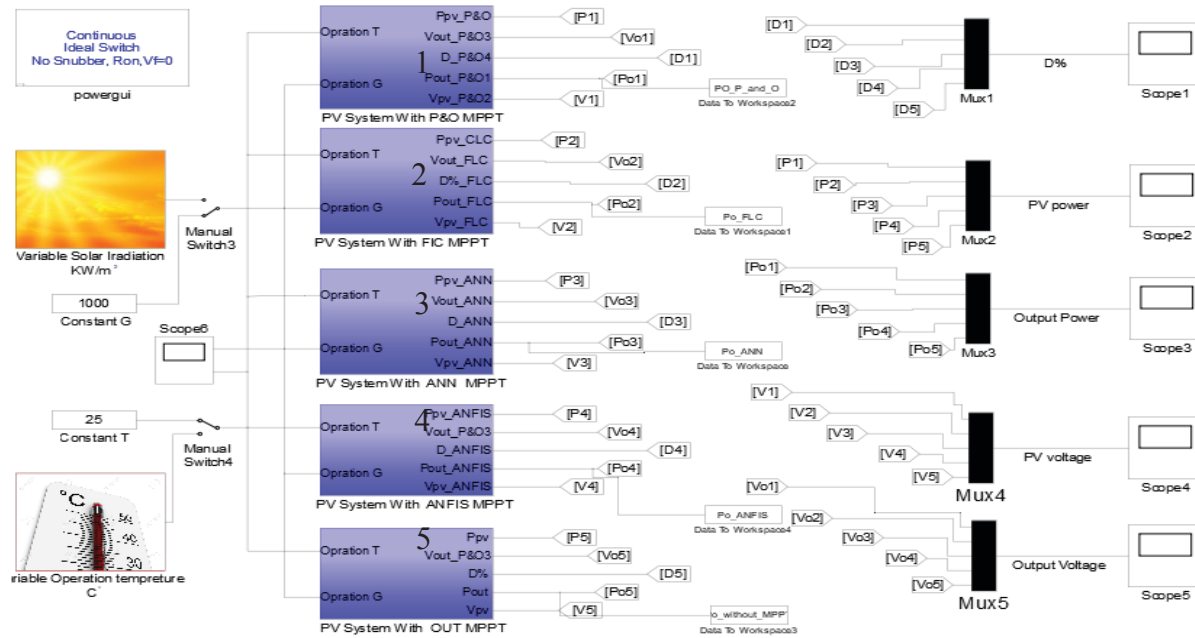
Figure 19. The simulation circuit of all PV systems for evaluating the performance of each MPPT

5.1 Simulation results

The simulation results are given in Figure 20 for the case varying in operation solar radiation value and in Figure 21 for the case varying in operation temperature value.

(a)

(b)

(c)
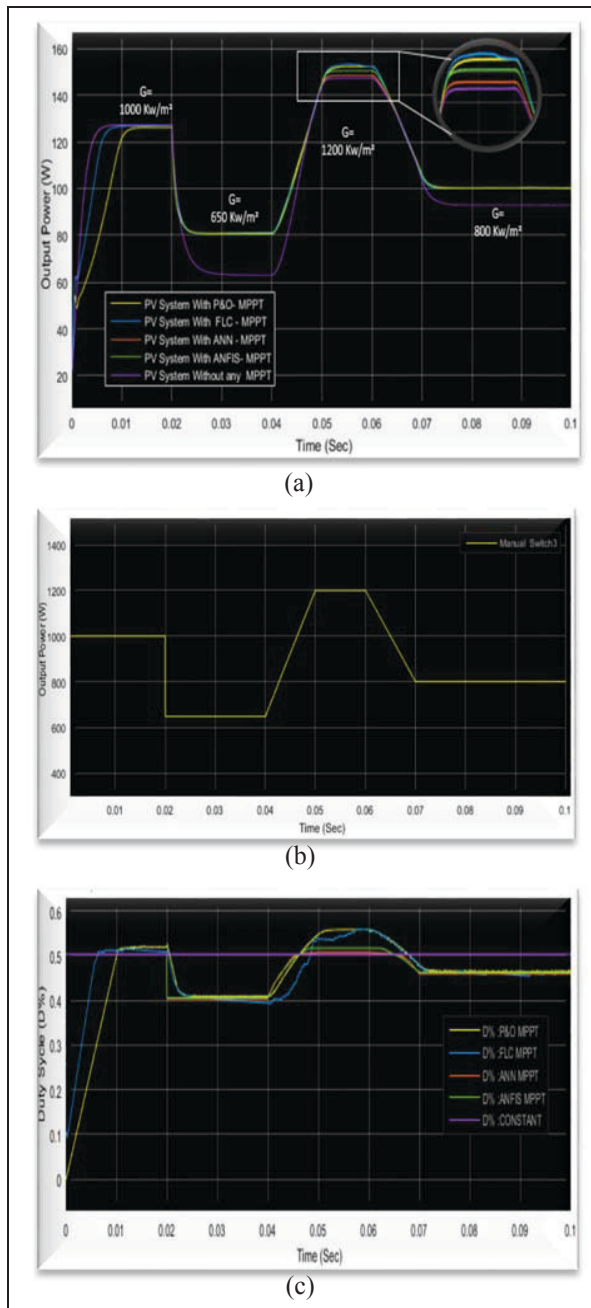
Figure 20. Simulations results for variation in G. (a) Output power of PV systems, (b) Solar irradiation variation signal, (c) Duty cycle decisions.

(a)

(b)

(c)

Figure 21. Simulations results for variation in T. (a) Output power of PV systems, (b) Solar irradiation variation signal, (c) Duty cycle decisions.

6.   Conclusion

As it is also seen in literatures and our simulation results, we conclude that the output power of the PV system which does not operate with MPPT, is less than the output power of the other PV systems which work with MPPT technique. Approximately 25% of the expected power is lost. For the system which works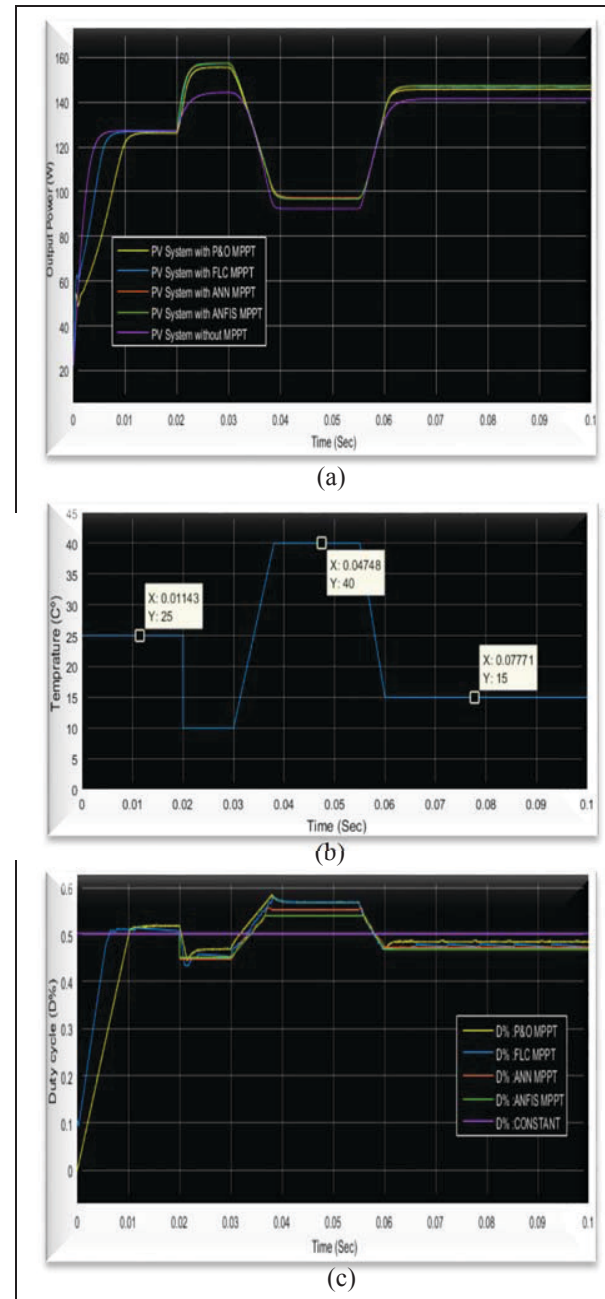 with the conventional P&O MPPT, we conclude that the time response for tracking MPP is slow and the MPP operation has less efficiency than the other systems. For the system which operates with MPPT based FLC, the time response for tracking the MPP is faster than P&O MPPT method and also more efficient for tracing MPP. For the MPPT based ANN and ANFIS; these techniques have the fastest time response for tracking the MPP and have a high efficiency for delivering the maximum power to the load.

See Table 4; summarizing the performances of the five different PV systems.

Table 4. Comparing the results of the purposed MPPT algorithms

Type of PV System	System Classification type	Control Sensors	MPPT Complexity	Time Response	Efficiency
Without MPPT	Without MPPT	NON	NON	Normal	75.6%
With P&O MPPT	Direct MPPT	I- PV AND V PV	Simple	Slow ,0.0142 Sec	97.43%
With FLC MPPT	Direct MPPT	I-PV AND V-PV	Average	Fast ,0.0094 Sec	98%
With ANN MPPT	Indirect MPPT	T and G	Complex	Fast,0.008 Sec	98.28%
With ANFIS MPPT	Indirect MPPT	T and G	Complex	Fast ,0.007 Sec	98.88%

Notes: From Figure 20 (a) note that the output power time is between 0.05 Sec and 0.06 Sec where the solar radiation is equal to 1200 Kw/m² ; the efficient MPPT, as it is seen is the MPPT based FLC, then comes the P&O MPPT, then comes the MPPT based ANFIS and then MPPT based ANN. However, in Figure 21 (a) note that the output power time is between 0.4 Sec and 0.05 Sec where the operation temperature is 40 Cº and all the results are equal.

The reasons which make the MPPT based ANN and MPPT based ANFIS are not efficient in this position; those two methods are indirect MPPT algorithms which make the decision of duty cycle based on the given values of G and T. ANN and ANFIS have been learning from the data that contains the situation of the system that operates in the range of G between 600 Kw/m² to 1100 Kw/m² and T from 10 to 30. So, the ANN and ANFIS do not give the right decision for a situation that they have not learned before the training process hence they give decisions that is close to the right decision. Therefore, the training process must be repeated with the training data that contains the new situation samples of G and T.

References

[1]. Foster, Robert, Majid Ghassemi, and Alma Cota. *Solar energy: renewable energy and the environment*. CRC Press, 2009.

[2]. Pelc, Robin, and Rod M. Fujita. "Renewable energy from the ocean." *Marine Policy* 26.6 (2002): [471-479].

[3]. Khaligh, A., and O. C. Onar. "Energy harvesting: solar, wind, and ocean energy conversion systems 2009."

[4]. Luque, Antonio, and Steven Hegedus, eds. *Handbook of photovoltaic science and engineering*. John Wiley & Sons, 2011.

[5]. Aribisala, Henry A. "Improving the efficiency of solar photovoltaic power system." (2013). http://digitalcommons.uri.edu/theses/161.

[6]. Esram, Trishan, and Patrick L. Chapman. "Comparison of photovoltaic array maximum power point tracking techniques." *IEEE Transactions on energy conversion* 22.2 (2007): [439-449].

[7]. Faranda, Roberto, and Sonia Leva. "Energy comparison of MPPT techniques for PV Systems." *WSEAS transactions on power systems* 3.6 (2008): [446-455].

[8]. Mukund R. Patel, *Design, Analysis, and Operation Wind and Solar Power Systems,* Published in 2006 by CRC Press Taylor & Francis Group, Boca Raton, FL [33487-2742].

[9]. Goetzberger, Adolf, and Volker Uwe Hoffmann. *Photovoltaic solar energy generation*. Vol. 112. Springer Science & Business Media, 2005.

[10]. Hasan Mahamudul, Mekhilef Saad, and Metselaar Ibrahim Henk. "Photovoltaic System Modeling with Fuzzy Logic Based Maximum Power Point Tracking Algorithm." *International Journal of Photo energy* 2013.

[11]. Faranda, Roberto, and Sonia Leva. "Energy comparison of MPPT techniques for PV Systems." *WSEAS transactions on power systems* 3.6 (2008): [446-455].

[12]. Sadek, Sahar M., et al. "Fuzzy P & O Maximum Power Point Tracking Algorithm for a Stand-Alone Photovoltaic System Feeding Hybrid Loads." *Smart Grid and Renewable Energy* 5.02 (2014): 19.

[13]. Zainudin, Hairul Nissah, and Saad Mekhilef. "Comparison study of maximum power point tracker techniques for PV systems." (2010).

[14]. Dolara, A., R. Faranda, and S. Leva. "Energy comparison of seven MPPT techniques for PV systems." *Journal of Electromagnetic Analysis and Applications* (2009).

[15]. Saleh Elkelani Babaa, Matthew Armstrong, Volker Pickertm "*Overview of Maximum Power Point Tracking Control Methods for PV Systems*" Journal of Power and Energy Engineering, [2014, 2, 59-72]

[16]. Sivagamasundari, M. S., P. Melba Mary, and V. K. Velvizhi. "Maximum power point tracking for photovoltaic system by perturb and observe method using buck boost converter." *International Journal of Advanced Research in Electrical, Electronics and Instrumentation Engineering* 2.6 (2013): [2433-2439].

[17]. Bendib, Boualem, Hocine Belmili, and Fateh Krim. "A survey of the most used MPPT methods: Conventional and advanced algorithms applied for photovoltaic systems." *Renewable and Sustainable Energy Reviews* 45 (2015): [637-648].

[18]. Yang, Shih-Ming, Y. J. Tung, and Y. C. Liu. "A NEURO-FUZZY SYSTEM DESIGN METHODOLOGY FOR VIBRATION CONTROL." *Asian Journal of control* 7.4 (2005): [393-400].

[19]. Ahmed, Jubaer, and Zainal Salam. "A Modified P&O Maximum Power Point Tracking Method with Reduced Steady-State Oscillation and Improved Tracking Efficiency." *IEEE Transactions on Sustainable Energy* 7.4 (2016): 1506-1515.

[20]. Femia, Nicola, et al. "Optimization of perturb and observe maximum power point tracking method." *IEEE transactions on Power Electronics* 20.4 (2005): [963-973].

[21]. Zainuri, Muhammad Ammirrul Atiqi Mohd, et al. "Development of adaptive perturb and observe-fuzzy control maximum power point tracking for photovoltaic boost dc–dc converter." *IET Renewable Power Generation* 8.2 (2013): [183-194].

[22]. David Sanz Morales, "*Maximum Power Point Tracking Algorithms for Photovoltaic Applications*", Faculty of Electronics, Communications and Automation. Espoo 14.12.2010.

[23]. Harjai, Arjav, Abhishek Bhardwaj, and Mrutyunjaya Sandhibigraha. *Study of maximum power point tracking (MPPT) techniques in a solar photovoltaic array*. Diss. 2011.

[24]. Marian Raducu, Hoarcă Ioan Cristian,"Maximum power point tracking algorithms", ECAI 2014 - International Conference – 6th Edition Electronics, Computers and Artificial Intelligence 23 October -25 October 2014, Bucharest, ROMÂNIA

[25]. Demuth, Howard B., et al. *Neural network design*. Martin Hagan,2014.

[26]. Prof. Laxmidhar Behera, "Electrical - Intelligent Systems and Control course" YouTube Lectures, Department of Electrical Engineering, Indian Institute of Technology, Kanpur. https://www.youtube.com/playlist?list=PL080F1A848428C3FD.

[27]. Bin-Halabi, Ahmed, Adel Abdennour, and Hussein Mashaly. "An Accurate ANFIS-based MPPT for Solar PV System." *International Journal of Advanced Computer Research* 4.2 (2014): 588.

[28]. M.Balaji Naik, Dr.P.Sujatha , "Adaptive fuzzy & Neuro-Fuzzy Inference controller based MPPT for photovoltaic systems", International Research Journal of Engineering and Technology (IRJET), Volume: 02 Issue: 08 | Nov-2015.

[29]. Jang, J-SR. "ANFIS: adaptive-network-based fuzzy inference system." *IEEE transactions on systems, man, and cybernetics* 23.3 (1993): [665-685].

[30]. Sarikaya, Nurcan, Kerim Guney, and Celal Yildiz. "Adaptive neuro-fuzzy inference system for the computation of the characteristic impedance and the effective permittivity of the micro-coplanar strip line." *Progress in Electromagnetics Research B* 6 (2008): 225-237.

[31]. Peter Vas, "ARTIFICAL INTELLIGENT -BASED ELECTRICAL MACHIN AND DEVICES" , ,published in United States by Oxford university Press ,Inc, New York ©Peter Vas 1999, https://books.google.com.tr/books?id=16Ai4r7qjuIC&printsec=frontcover&hl=ar#v=onepage&q&f=false.

[32]. Iqbal, A., H. Abu-Rub, and Sk M. Ahmed. "Adaptive neuro-fuzzy inference system based maximum power point tracking of a solar PV module." *Energy Conference and Exhibition (EnergyCon), 2010 IEEE International*. IEEE, 2010.

[33]. Daniel W. Hart "Power Electronics", Book Published by McGraw- Companies, [TK7881.15.H373 2010 621.31'7—dc22], http://www.mheducation.com

[34]. Marańda, Witold, and Maciej Piotrowicz. "Efficiency of maximum power point tracking in photovoltaic system under variable solar irradiance." *Bulletin of the Polish Academy of Sciences Technical Sciences* 62.4 (2014): [713-721].

[35]. Rahim, Nasrudin Abd, Hew Wooi Ping, and Jeyraj Selvaraj. "Photovoltaic module modeling using Simulink/Matlab." *Procedia Environmental Sciences* 17 (2013): [537-546].

[36]. Koivo, Heikki N. "Neural networks: Basics using matlab neural network toolbox." *Author Website* (2008).

SUBMISSION INSTRUCTIONS

The scope of International Journal of Electronics, Mechanical and Mechatronics Engineering (IJEMME) covers the novel scientific papers about Electronics, Image Processing, Information Theory, Electrical Systems, Power Electronics, Control Theory, Embedded Systems, Robotics, Motion Control, Stochastic Modeling, System Design, Multidisciplinary Engineering, Computer Engineering, Optical Engineering, Design Optimization, Material Science, Metamaterials, Heat and Mass Transfer, Kinematics, Dynamics, Thermo-Dynamics, Energy and Applications, Renewable Energy, Environmental Impacts, Structural Analysis, Fluid Dynamics and related topics of the above subjects.

IJEMME is an international periodical published triple a year (February, July and October). Manuscripts reporting on original theoretical and/or experimental work and tutorial expositions of permanent reference value are welcome. IJEMME Editorial Board is authorized to accept/reject the manuscripts based on the evaluation of international experts. The papers should be written in English.

The manuscript should be sent in electronic submission via **zaferutlu@aydin.edu.tr**

SUBMISSION INSTRUCTIONS OF MANUSCRIPTS.

Page Design: Text body area is (195mm x 275mm). 30 mm margin from top, 20 mm from down and 25 mm margin should be left on right/left sides.

Title: should be in 16 pt. bold, capital letters with Times New Roman font in Microsoft Word format. Authors' names, affiliations, e-mail addresses should follow the title after double line spacing with authors' names and surnames in lower case except first letters in 14 pt, the rest is 10 pt. italic.

Abstract: should not exceed 200 words with the word "Abstract" in 10 pt. italic, bold, abstract text in 9 pt. italic, all in Times New Roman font in Microsoft Word format.

Keywords: not exceeding 5 should be in bold.

Document Character: Subtitles should be in 10 pt. bold, capital letters and text body 10 pt. both with Times New Roman font in Microsoft Word format. The manuscripts should be written on a single column, be double spaced with single line spacing between paragraphs. The subtitle of the first section should start after a single space following the keywords, the other subtitles also with a single line space following the text, there should also be single line spacing between the previous text and the subtitle.

CONCLUSION section should have a title written in 1o pt. bold, capital letters and the text in 10 pt. all in Times New Roman font in Microsoft Word format.
REFERENCE numbers should be given in brackets as illustrated below:
Referencing books:

[1] Özsu M., T, Valduriez, P., Principles of Distributed Database Systems, Prentice Hall, New Jersey, 128-136,1991.

Referencing papers:

[2] G. Altay, O. N., Ucan, "Heuristic Construction of High-Rate Linear Block Codes," International Journal of Electronics and Communications (AEU), vol. 60, pp.663-666, 2006.

Page number is to be placed at the top left corner of each page with pencil.
Length of the Manuscript should not exceed 20 pages excluding Figures and Tables.

INSTRUCTIONS ABOUT THE ACCEPTED MANUSCRIPTS:
Page Design: Text body area is (195mm x 275mm). 30 mm margin from top, 20 mm from down and 25 mm margins should be left on right/left sides.

Title: should be in 16 pt. bold, capital letters with Times New Roman font in Microsoft Word format. Authors' names, affiliations, e-mail addresses should follow the title after double line spacing with authors' names in lower case and surnames in capital letter in 14 pt. the rest in 10 pt. in the same format.

Abstract: should not exceed 200 words with the word "Abstract" in 12 pt. italic, bold, abstract text in 9 pt. italic, all in Times New Roman font in Microsoft Word format.

Keywords: not exceeding 5 should be in 9 pt. bold.

Document Character: Subtitles should be in 10 pt. bold, capital letters and text body 10 pt. both with Times New Roman font in Microsoft Word format. **The manuscripts should be written on two columns, be single spaced with single line spacing between paragraphs.** The subtitle of the first section should start after a single space following the keywords, the other subtitles also with a single line space following the text, there should also be single line spacing between the previous text and the subtitle.

SECTIONS: Formulas should be numbered sequentially. Referring to formulas should be as Eqn (.). Figures and Tables should be placed into the text body and captions for both should be 10 pt. Table numbers and captions should be placed before the Table. If necessary, both columns may be used for large Figures and Tables.

CONCLUSION section should have a title written in 12 pt. bold, capital letters and the text in 10 pt. all in Times New Roman font in Microsoft Word format. Conclusion should not be a version of the Abstract.
REFERENCE numbers should be given in brackets as illustrated below:

Referencing books:
[1] Özsu M., T, Valduriez, P., Principles of Distributed Database Systems, Prentice Hall, New Jersey, 128-136,1991.

Referencing papers:

[2]G. Altay, O. N., Ucan, "Heuristic Construction of High-Rate Linear Block Codes," International Journal of Electronics and Communications (AEU), vol. 60, pp.663-666, 2006.

SHORT BIOGRAPHY of the authors should follow references after a single line space, names in 9 pt. surnames in 9 pt. and the text in 9 pt. The text should not exceed 100 words.

CORRESPONDENCE ADDRESS:

Editor
Prof. Dr. Zafer UTLU
Engineering Faculty
Mechanical Engineering Department
Inonu Caddesi, No.38, Florya, Istanbul, TURKEY
E-mail: zaferutlu@aydin.edu.tr
Web : www.aydin.edu.tr/eng/ijemme

Prepared by
Instructor: Şenay KOCAKOYUN
Anadolu BIL Vocational High School
Computer Programming Department
Inonu Caddesi, No.38 Florya, Istanbul, TURKEY
E-mail: senaykocakoyun@aydin.edu.tr

Published by
Istanbul Aydın University